HHS Public Access

Author manuscript

Nat Microbiol. Author manuscript; available in PMC 2021 January 13.

Published in final edited form as:

Nat Microbiol. 2020 October ; 5(10): 1271–1284. doi:10.1038/s41564-020-0756-3.

Lactate production by *Staphylococcus aureus* biofilm inhibits HDAC11 to reprogram the host immune response during persistent infection

Cortney E. Heim[1], **Megan E. Bosch**[1,‡], **Kelsey J. Yamada**[1], **Amy L. Aldrich**[1,#], **Sujata S. Chaudhari**[1], **David Klinkebiel**[2,4], **Casey M. Gries**[1,&], **Abdulelah A. Alqarzaee**[1], **Yixuan Li**[5], **Vinai C. Thomas**[1], **Edward Seto**[5], **Adam R. Karpf**[3,4], **Tammy Kielian**[1,*]

[1]Department of Pathology and Microbiology, University of Nebraska Medical Center, Omaha, NE 68198;

[2]Department of Biochemistry and Molecular Biology, University of Nebraska Medical Center, Omaha, NE 68198;

[3]Department of Eppley Institute, University of Nebraska Medical Center, Omaha, NE 68198;

[4]Department of Fred and Pamela Buffett Cancer Center, University of Nebraska Medical Center, Omaha, NE 68198;

[5]Department of Biochemistry & Molecular Medicine, George Washington University School of Medicine & Health Sciences, Washington, DC 20037

Abstract

Staphylococcus aureus (*S. aureus*) is a leading cause of biofilm-associated prosthetic joint infection (PJI), resulting in significant disability and prolonged treatment. It is known that host leukocyte IL-10 production is required for *S. aureus* biofilm persistence in PJI. A *S. aureus bursa aurealis* Tn library consisting of 1,952 non-essential genes was screened for mutants that failed to

*Corresponding Author: Tammy Kielian, Ph.D., University of Nebraska Medical Center, Department of Pathology and Microbiology, 985900 Nebraska Medical Center, Omaha, NE 68198-5900, Phone: (402) 559-8002, FAX: (402) 559-5900, tkielian@unmc.edu.
‡Current address: Department of Neurology, Washington University School of Medicine, St. Louis, MO 63110
#Current address: Moffitt Cancer Center, Tampa, FL 33612
&Current address: Division of Biomedical Sciences, University of California Riverside School of Medicine, Riverside, CA, 92521

AUTHOR CONTRIBUTIONS

CEH and TK conceived the study, CEH, MEB, KJY, ALA, and TK designed experiments, and ARK and DK provided expertise in the design, execution, and data analysis for the ChIP-seq, ChIP-PCR, and scRNA-seq experiments. SSC, AAA, CMG, and VCT created the *S. aureus* lactate mutants used in the study. CEH, MEB, KJY, and ALA conducted the *in vivo* mouse PJI experiments. CEH performed the *in vitro* biofilm-leukocyte co-culture experiments. ES and YL provided the HDAC11 KO mice. CEH, DK, and TK performed data analysis. TK procured funding for this work. CEH and TK wrote the manuscript. All authors edited and approved the submission of this work.

COMPETING INTERESTS

The authors declare no competing interests.

DATA AVAILABILITY

The ChIP-seq and RNA-seq datasets are available in the GEO repository (accession number GSE135496) and Source Data is provided for the main figures and Extended Data in this study.

CODE AVAILABILITY

All codes utilized are published programs, with links to each provided in the Methods.

induce IL-10 in myeloid-derived suppressor cells (MDSCs), which identified a critical role for bacterial lactic acid biosynthesis. We generated a *S. aureus ddh/ldh1/ldh2* triple Tn mutant that cannot produce D- or L-lactate. Co-culture of MDSCs or macrophages with *ddh/ldh1/ldh2* mutant biofilm produced substantially less IL-10 compared with wild type *S. aureus*, which was also observed in a mouse model of PJI and led to reduced biofilm burden. Using MDSCs recovered from the mouse PJI model and *in vitro* leukocyte-biofilm co-cultures we show that bacterial-derived lactate inhibits histone deacetylase 11 (HDAC11), causing unchecked HDAC6 activity and increased histone 3 acetylation at the *Il-10* promoter, resulting in enhanced *Il-10* transcription in MDSCs and macrophages. Finally, we show that synovial fluid of patients with PJI contains elevated amounts of D-lactate and IL-10 compared with control subjects, and bacterial lactate increases IL-10 production by human monocyte-derived macrophages.

SUMMARY PARAGRAPH

Biofilms are bacterial communities that are difficult to treat because of their tolerance to antibiotics and ability to evade immune-mediated clearance. Prosthetic joint infection (PJI), a devastating complication of arthroplasty, is characterized by biofilm formation. The current study has discovered a central role for lactic acid biosynthesis in *S. aureus* biofilm formation during PJI. Mechanistically, bacterial-derived lactate inhibits histone deacetylase 11 (HDAC11) activity, which causes extensive epigenetic changes at the promoters of numerous host genes, including the key anti-inflammatory cytokine *Il-10*. Indeed, IL-10 production by myeloid-derived suppressor cells (MDSCs) and macrophages is critical for biofilm persistence during PJI. HDAC11 inhibition by *S. aureus* lactate results in unchecked HDAC6 activity, a positive regulator of IL-10, thereby increasing IL-10 production by MDSCs and macrophages *in vitro* and *in vivo*. Similarly, *S. aureus* lactate promotes IL-10 production in human monocyte-derived macrophages following biofilm exposure. This study highlights how bacterial metabolism can influence the host immune response to promote infection persistence.

Keywords

S. aureus; lactate; biofilm; interleukin-10; myeloid-derived suppressor cell; macrophage; histone deacetylase; prosthetic joint infection

INTRODUCTION

Staphylococcus aureus (*S. aureus*) is a leading cause of implanted medical device infections, characterized by biofilm formation[1–3]. Bacterial biofilms are microbial communities that exhibit distinct metabolic properties that contribute to their chronicity and antibiotic tolerance[4–6]. Staphylococcal biofilms actively reprogram the host innate immune response to favor persistent infection[7–13]. This is mediated, in part, by the recruitment of myeloid-derived suppressor cells (MDSCs) that promote monocyte and macrophage anti-inflammatory properties[14–17]. In addition, *S. aureus* biofilm evades Toll-like receptor (TLR)-mediated recognition and inhibits macrophage phagocytosis[7,10,18]. Collectively, these mechanisms lead to biofilm persistence.

IL-10 is a potent anti-inflammatory cytokine[19] and although it is critical for preventing excessive pro-inflammatory responses and immunopathology associated with some types of infections, dysregulated or mistimed IL-10 production can allow select pathogens to escape immune control, resulting in chronic infection[16,20–22]. It is well recognized that IL-10 inhibits T cell activation and Th1 polarization[23–25], and MDSCs have been shown to engage in crosstalk with macrophages, in part via IL-10, to skew them toward an anti-inflammatory phenotype during tumor growth[26,27]. We have previously shown that MDSCs are the main source of IL-10 during early *S. aureus* biofilm infection, transitioning to monocytes at later stages, and IL-10 production contributes to infection persistence[16].

Based on the importance of IL-10 in promoting biofilm infection, we screened the Nebraska Transposon Mutant Library (NTML)[28] to identify *S. aureus* factors that stimulate IL-10 production by MDSCs and macrophages. Numerous genes involved in lactate biosynthesis were identified, suggesting that bacterial lactate is an important regulator of leukocyte activation. Lactate is a product of glycolysis that exists as two stereoisomers, L- and D-lactate. *S. aureus* encodes three lactate biosynthetic enzymes, including an inducible L-lactate dehydrogenase (Ldh1), a second L-lactate dehydrogenase (Ldh2), and a D-lactate dehydrogenase (Ddh)[29,30], to produce both L- and D-lactate, respectively. In eukaryotes, L-lactate is the predominant metabolite, whereas D-lactate is present at very low concentrations[31]. Recently, lactate has been implicated in mechanisms of immune evasion[32–34], including inhibition of monocyte and macrophage cytokine production[35].

Lactate has been reported to influence chromatin function and gene expression by inhibiting histone deacetylase (HDAC) activity in immune cells[36,37]; however, the role of HDACs, and more specifically how they are regulated in leukocytes in the context of biofilm infection, has not been investigated. Histones are a class of highly conserved proteins (H3, H4, H2A, H2B, and H1) that are integral for regulating gene transcription through post-translational modifications of N-terminal histone tails, including methylation, phosphorylation, lactylation, and acetylation[34,38]. Histone acetylation is mediated by histone acetyltransferases that transfer an acetyl group to a lysine residue on the histone tail, which relaxes chromatin structure and increases promoter accessibility and gene transcription. Deacetylation is mediated by HDACs, which condense chromatin and favor gene silencing[39]. There are 18 HDACs in humans that are grouped into four families, including Class I (HDAC1, −2, −3, and −8), Class II (HDAC4, −5, −6, −7, −9, and −10), Class III (sirtuins; SIRT1, −2, −3, −4, −5, −6 and −7), and Class IV (HDAC11)[39]. HDAC6 and HDAC11 physically interact and have been identified as positive and negative regulators of *IL-10* transcription, respectively[40,41]. In this report, we demonstrate that *S. aureus* biofilm-derived lactate inhibits HDAC11 to augment *IL-10* transcription via unchecked HDAC6 activity, which promotes the anti-inflammatory properties of MDSCs and macrophages. Since lactate biosynthesis is a conserved pathway in bacteria[42–45], this study highlights the potential broader implications of lactate as a regulator of leukocyte gene expression during infections caused by diverse bacterial species.

RESULTS

S. aureus lactate biosynthesis pathways induce IL-10 production by MDSCs and macrophages.

To determine whether *S. aureus*-derived factors are responsible for eliciting IL-10 production from MDSCs, we designed a screen of the NTML, a collection of 1,952 strains each possessing a single mutation of a nonessential gene in *S. aureus* strain USA300 JE2[28]. This approach identified several hits in the *S. aureus* lactate biosynthesis pathway that were attenuated in their ability to elicit IL-10 production from MDSCs, namely Δ*ddh*, Δ*ldh1*, and Δ*ldh2*, which convert pyruvate to D- and L-lactate, respectively (Figure 1a; Extended Data 1a). Because L-lactate production in *S. aureus* is driven by two independent genes[29], we created a Δ*ldh1/ldh2* as well as Δ*ddh/ldh1/ldh2* that lacks all lactate biosynthetic enzymes. Importantly, these lactate mutants showed no growth defects in liquid broth or biofilm (Extended Data 1b and c). Both Δ*ldh1/ldh2* and Δ*ddh/ldh1/ldh2* biofilm produced negligible L-lactate (Figure 1c) and D-lactate was undetectable in Δ*ddh* and Δ*ddh/ldh1/ldh2* biofilm (Figure 1d). Both MDSCs and macrophages produced significantly less IL-10 when co-cultured with Δ*ddh*, Δ*ldh1/ldh2*, or Δ*ddh/ldh1/ldh2* biofilm compared to WT (Figure 1b). The intracellular pH of leukocytes co-cultured with WT or Δ*ddh/ldh1/ldh2* biofilm was similar, revealing that pH fluctuations were not a contributing factor for lactate effects (Extended Data 2).

IL-10 production by both MDSCs and macrophages in response to Δ*ddh,* Δ*ldh1/ldh2* or Δ*ddh/ldh1/ldh2* biofilm could be partially restored with exogenous sodium D- or L-lactate (Figure 1e). However, a Δ*ddh* and Δ*ldh1/ldh2* mixed biofilm returned MDSC and macrophage IL-10 production to levels elicited by WT biofilm (Figure 1f), a scenario where both D- and L-lactate are present. The mechanism of lactate release from *S. aureus* biofilm appears to be mediated by the lactate permease *lctP1*[46], since a Δ*lctP1* biofilm also elicited less IL-10 production by MDSCs and macrophages (Supplementary Figure 1). The majority of lactate transport in mammalian cells occurs via the family of proton-linked monocarboxylate transporters (MCTs)[47]. Of this family, MCT1 is ubiquitously expressed and mediates bi-directional transport of monocarboxylates, including L- and D-lactate[47–49]. AZD3965[47] and 7ACC2[50] are selective MCT1 inhibitors, and both significantly decreased IL-10 production by MDSCs and macrophages following co-culture with WT *S. aureus* biofilm (Figure 1g).

S. aureus-derived lactate promotes bacterial persistence during PJI in an IL-10-dependent manner.

We next examined the course of biofilm infection with WT, Δ*ddh*, Δ*ldh1/ldh2*, and Δ*ddh/ldh1/ldh2* in a mouse orthopaedic implant model. Bacterial burden in implant-associated tissue was significantly decreased for all three mutants at days 14 and 28 post-infection (Figure 2a). This coincided with fewer MDSCs and increased neutrophil and monocyte infiltrates at days 14 and 28 post-infection (Figure 2c–g); furthermore, as expected, lactate levels were reduced in animals infected with the lactate mutants at these intervals (Extended Data 3). Interestingly, only Δ*ldh1/ldh2* and Δ*ddh/ldh1/ldh2* were reduced in the femur at days 14 and 28, indicating an L-lactate-dependent phenotype in the bone (Figure 2b).

Although IL-10 expression trended lower across the entire time course with all of the lactate mutants, IL-10 levels were not significantly decreased until day 28 in the absence of both *S. aureus* D- and L-lactate (Δ*ddh/ldh1/ldh2*; Figure 2h). This reduction in IL-10 was likely lactate-dependent and not influenced by decreased bacterial burden at this time point, since the expression of other inflammatory mediators was similar in WT and Δ*ddh/ldh1/ldh2* infected tissues, as well as MDSCs and monocytes isolated from WT and Δ*ddh/ldh1/ldh2* infected mice at day 28 post-infection (Extended Data 4 and Supplementary Table 1, respectively). During acute infection (day 3), both MDSCs and monocytes recovered from Δ*ddh/ldh1/ldh2*-infected mice expressed less IL-10 mRNA compared to WT *S. aureus* (Figure 2i). In addition, TNF-α expression was increased in monocytes from Δ*ddh/ldh1/ldh2*-infected mice concomitant with a reduction in the anti-inflammatory marker Arg-1 (Figure 2i), suggesting that monocytes are more pro-inflammatory in the absence of bacterial lactate. The Δ*ddh/ldh1/ldh2* strain was utilized for all subsequent experiments to assess the biological impact of *S. aureus* lactate on leukocyte activation.

Co-infection with WT and Δ*ddh/ldh1/ldh2* reversed the immune phenotypes associated with Δ*ddh/ldh1/ldh2* monoinfection, including a return of IL-10 production (Figure 3f) and leukocyte infiltrates (Figure 3c–e) as well as D- and L-lactate (Figure 3g and h) to WT levels at days 14 or 28 post-infection, supporting the action of bacterial-derived and not host lactate. The titer of Δ*ddh/ldh1/ldh2* during co-infection was comparable to monoinfection; revealing that WT bacteria did not outcompete Δ*ddh/ldh1/ldh2* over the 28-day co-infection period (Figure 3a and b). To determine whether the residual IL-10 production after infection with Δ*ddh/ldh1/ldh2* reflected the action of host lactate, mice were treated with sodium oxamate, a LDH inhibitor that has been used in cancer models[51–53]. Oxamate treatment of Δ*ddh/ldh1/ldh2* infected mice had no effect on IL-10 production (Extended Data 5), demonstrating that *S. aureus*-derived lactate is the main driver of IL-10 expression during biofilm infection, confirming the co-infection experiments (Figure 3). Oxamate did not alter *S. aureus* growth or lactate production (Extended Data 6c–e). We also examined whether IL-10 was elicited by pathogen-associated molecular patterns in the biofilm, which in *S. aureus* primarily signal via TLRs 2 and 9 and utilize the adaptor protein MyD88[54–56]. IL-10 production by both MDSCs and macrophages following co-culture with WT biofilm was MyD88- and TLR2-independent (Supplementary Figure 2), emphasizing the critical role of biofilm-derived lactate in inducing IL-10 expression.

To confirm that the effects of *S. aureus*-derived lactate *in vivo* were mediated by IL-10, IL-10 KO and WT mice were infected with WT *S. aureus* or Δ*ddh/ldh1/ldh2*. We previously reported that bacterial burden and MDSC infiltrates were significantly reduced at day 14 post-infection in IL-10 KO mice infected with WT *S. aureus*[16], which was confirmed here (Extended Data 7a–c). In contrast, reduction in bacterial titer and changes in MDSC and monocyte infiltrates in WT mice following Δ*ddh/ldh1/ldh2* infection were not observed in IL-10 KO animals (Extended Data 7), indicating that the main effects of *S. aureus*-derived lactate are IL-10-dependent.

S. aureus-derived lactate inhibits HDAC11, resulting in unchecked HDAC6-driven IL-10 production.

In eukaryotic cells, lactate can regulate gene transcription by inhibiting HDACs[36,37] and the *IL-10* promoter can be regulated by histone acetylation[40,41,57,58]. It is unknown whether *S. aureus*-derived lactate can affect HDACs, which would represent a metabolic virulence determinant. HDAC activity was significantly decreased in leukocytes recovered from WT compared to Δ*ddh/ldh1/ldh2* infected mice (Figure 4a) and coincided with increased total histone 3 acetylation (H3Ac; Figure 4b), consistent with the action of *S. aureus* lactate as an HDACi. This was further supported by ChIP-seq, where total H3Ac within ± 10,000 bp of all genomic transcription start sites was increased by approximately two-fold in MDSCs recovered from mice infected with WT *S. aureus* vs. Δ*ddh/ldh1/ldh2* (Figure 4c). scRNA-seq of $CD45^+$ leukocytes isolated from WT and Δ*ddh/ldh1/ldh2* infected mice identified several genes with concordant changes in H3Ac status and transcriptional expression, including *IL-10*, where acetylation and gene expression were both reduced in response to Δ*ddh/ldh1/ldh2* (Figure 4d), independently confirming the findings of increased IL-10 levels in the setting of WT *S. aureus* infection. Other notable changes were increases in pro-inflammatory and bactericidal genes in Δ*ddh/ldh1/ldh2*-infected mice, such as cathepsin (*Ctsg*) and myeloperoxidase (*Mpo*), whereas several genes associated with MDSC recruitment and immunosuppression (*IFNb1*, *Nfkbiz*, *Cxcl1*, *Cxcl3*, *Fpr1*, and *Ptgs2*) were reduced (Figure 4d)[59–64]. Also of interest was reduced MCT1 (*Slc16a1*) expression in Δ*ddh/ldh1/ldh2*-infected mice, suggesting that lactate production by WT *S. aureus* augments MCT1 expression to promote lactate uptake and IL-10 production. The concordance between H3Ac levels and gene expression identified by ChIP-seq was validated by RT-qPCR (Figure 4e). ChIP-qPCR confirmed increased H3Ac in three regions near the *IL-10* promoter in leukocytes from WT-infected mice that were identified by ChIP-seq, i.e. −5795 TSS, +450 TSS, and the *STAT3* binding site at −507 TSS[65] (Figure 4f). Treatment of Δ*ddh/ldh1/ldh2* infected mice with the pan-HDACi trichostatin A (TSA) increased IL-10 production and bacterial burden to levels approaching that of WT *S. aureus* (Figure 4g–i). TSA had no effect in mice infected with WT *S. aureus*, which is expected if bacterial-derived lactate is already acting as an HDACi (Figure 4g–i).

HDAC6 has been shown to be a positive regulator of IL-10 production, whereas HDAC11 is a negative regulator that inhibits HDAC6[40,41]. If *S. aureus* lactate inhibits HDAC11, this might alleviate the negative feedback on HDAC6 at the *IL-10* promoter, effectively augmenting IL-10 production. To investigate this possibility, MDSCs and macrophages from HDAC11 KO and WT mice were co-cultured with *S. aureus* biofilm. HDAC11 KO leukocytes produced significantly more IL-10 in response to Δ*ddh/ldh1/ldh2* biofilm, which likely resulted from unchecked HDAC6 activity, since IL-10 was significantly reduced by the HDAC6i tubastatin A (Figure 5b). Tubastatin A treatment of WT leukocytes co-cultured with WT biofilm also significantly reduced IL-10 production (Figure 5a), reflecting unchecked HDAC6 activity following inhibition of the negative regulator HDAC11 by *S. aureus* lactate. This was supported by the lack of tubastatin A effects on WT leukocytes co-cultured with Δ*ddh/ldh1/ldh2* biofilm because the absence of lactate allowed HDAC11 to inhibit HDAC6 (Figure 5b). Similar results were obtained with a second HDAC6i (Extended Data 8). Cell-free experiments demonstrated that *S. aureus*-derived lactate preferentially

targeted HDAC11, since the degree of enzyme inhibition by WT biofilm was greater for HDAC11 than HDAC6, whereas conditioned medium from a Δ*ddh/ldh1/ldh2* biofilm was significantly less potent at blocking HDAC11 activity (Extended Data 9).

To investigate this mechanism *in vivo*, two complementary experiments were performed. Infection of WT and HDAC11 KO mice with WT *S. aureus* showed no significant differences in IL-10 production, leukocyte infiltrates, or bacterial burden (Figure 5c–h). This is expected if *S. aureus*-derived lactate inhibits HDAC11, making the loss of HDAC11 irrelevant, since nothing is inhibiting HDAC6 and thus IL-10 is already maximally expressed. In contrast, IL-10 production was significantly higher in HDAC11 KO mice infected with Δ*ddh/ldh1/ldh2* compared to WT animals (Figure 5h), likely due to the lack of negative regulation of HDAC11 on HDAC6 activity that drives IL-10 production, which translated into increased bacterial burden in implant-associated tissue (Figure 5c). To demonstrate HDAC6 action *in vivo*, WT mice were treated with tubastatin A. Bacterial burden in the implant-associated tissue and femur as well as IL-10 production were all significantly reduced in animals infected with WT *S. aureus* following tubastatin A treatment, a phenotype similar to when no *S. aureus* lactate is produced (Δ*ddh/ldh1/ldh2*; Figure 5i–k). Moreover, tubastatin A had no effect in Δ*ddh/ldh1/ldh2*-infected WT mice (Figure 5i–k), since HDAC6 was already being inhibited by HDAC11 in the absence of *S. aureus*-derived lactate. Importantly, IL-10 levels were similar in HDAC11 KO mice in response to WT or Δ*ddh/ldh1/ldh2* infection (Figure 5h) and total IL-10 was equivalent in WT and Δ*ddh/ldh1/ldh2* infected animals following HDAC6 inhibition (Figure 5k), since once HDAC6 is inhibited the lack of HDAC11 makes no difference. Collectively, these findings support the *in vitro* studies, showing that bacterial-derived lactate is an HDAC11i that augments IL-10 production during *S. aureus* biofilm infection, by alleviating the negative feedback on HDAC6.

Both D-lactate and IL-10 were significantly increased in the synovial fluid of human PJIs caused by distinct bacteria, including *S. aureus*, *S. epidermidis*, and Group C *Streptococcus*, compared to aseptic joints; whereas, L-lactate levels were similar (Figure 6a and b). In addition, human monocyte-derived macrophages treated with clarified supernatant from Δ*ddh/ldh1/ldh2* biofilm produced significantly less IL-10 than in the presence of lactate (Figure 6c), which was confirmed by L- and D-lactate quantification (Figure 6d and e). Similar to mouse macrophages, IL-10 production by human monocyte-derived macrophages was HDAC6-driven and lactate-dependent, since tubastatin A significantly decreased IL-10 levels following treatment with WT but not Δ*ddh/ldh1/ldh2* clarified biofilm supernatant (Figure 6c).

Collectively, these experiments demonstrate that *S. aureus*-derived lactate is transported into MDSCs and macrophages via MCT1. Through its action as an HDAC11i, bacterial lactate releases its negative regulation on HDAC6, a positive regulator of IL-10, resulting in increased IL-10 production during *S. aureus* biofilm infection (Figure 5l). Bacterial lactate also induces a global increase in H3Ac, reflecting mechanisms of epigenetic regulation extending beyond IL-10 that could also contribute to biofilm persistence.

DISCUSSION

It is well established that post-translational modifications of histones influence gene expression[34,38,66]. Here we demonstrate that D- and L-lactate, products of *S. aureus* fermentative metabolism, promote IL-10 production by biofilm-associated MDSCs and macrophages via HDAC11 inhibition. ChIP-seq and subsequent ChIP-qPCR identified the proximal region of the IL-10 promoter (−87 to −7) as a target of H3Ac by *S. aureus*-derived lactate, in agreement with a recent report[40]. This metabolic crosstalk is critical to sustain an anti-inflammatory environment that promotes bacterial persistence, demonstrating that a *S. aureus* metabolite can act as a virulence factor.

Recent reports have examined the role of HDAC11 in regulating MDSC expansion and function in the context of cancer[67–69]. MDSCs isolated from tumor-bearing mice displayed high HDAC11 expression compared to immature myeloid cells, and MDSCs from tumor-bearing HDAC11 KO mice were more suppressive with increased IL-10 levels, which was associated with enhanced tumor growth[69]. These observations share striking parallels to what was observed during *S. aureus* biofilm infection. IL-10 production was significantly higher in HDAC11 KO versus WT animals infected with Δ*ddh/ldh1/ldh2* due to the loss of this negative regulator. This allowed us to unveil the role of HDAC6 as a driver of IL-10 expression using selective HDAC6 inhibitors. Recent evidence suggests that although HDAC6 binds to the *IL-10* promoter and induces gene expression, it has minimal effects on histone deacetylation[40], which could explain the preferential inhibition of *S. aureus*-derived lactate on HDAC11 versus HDAC6, which was supported by cell-free assays. Furthermore, we showed that *S. aureus*-derived lactate promotes IL-10 production in human monocyte-derived macrophages through HDAC11i and increased HDAC6 activity, reflecting the translational impact of our findings.

The mechanism whereby *S. aureus* lactate inhibits HDAC11 remains elusive. Pathogen targeting of HDACs has been demonstrated for other bacteria, including *Mycobacterium tuberculosis*, *Helicobacter pylori*, and *Listeria monocytogenes* but via distinct mechanisms[70–73]. Recent studies have shown that HDAC11 has other enzymatic functions in addition to deacetylase activity[74–76]; therefore, it is likely that the effects of *S. aureus*-derived lactate on HDAC11 extend beyond promoting *IL-10* transcription. Furthermore, since the increase in HDAC activity during Δ*ddh/ldh1/ldh2* infection was greater in magnitude compared to changes in H3Ac levels, it is possible that the *S. aureus* lactate-dependent changes in HDAC activity have effects beyond transcriptional regulation. Recently, lactate has been reported to influence the post-translational modification of histones via a process termed histone lactylation[34]. It is unclear what impact histone lactylation may play in the setting of *S. aureus* biofilm infection and represents an area for future investigation.

Although this study focused on the ability of *S. aureus*-derived lactate to regulate IL-10 expression, lactate also altered H3Ac at other genes, reflecting a broader mechanism of action. Notable genes that were increased in leukocytes from Δ*ddh/ldh1/ldh2* mice included enzymes associated with neutrophil bactericidal activity (*Ctsg*, *Mpo*)[77,78], which correlated with reduced bacterial burden in the absence of lactate. In addition, the expression of genes

that have been linked to MDSC recruitment (*Cxcl1* and *Cxcl3*)[63,79] and suppressive activity (*Ptgs2*)[80] were decreased in the absence of *S. aureus* lactate, which agrees with the reduction in MDSC infiltrates in Δ*ddh/ldh1/ldh2*-infected animals. Although several of the genes detected by ChIP-seq are typically associated with T cells (i.e. granzymes, cathepsins) they are also expressed in MDSCs[81,82]. Our prior work has identified T cell infiltrates in patients with PJI as well as the mouse *S. aureus* PJI model, although they represent a minor population in both instances (i.e. < 2% of $CD45^+$ leukocytes)[15,83].

It remains unclear whether *S. aureus*-derived D- and L-lactate exert distinct functions in MDSCs and macrophages, since our results have revealed actions for both stereoisomers. The MCT-1 transporter that was important for eliciting *S. aureus* lactate-dependent IL-10 production is more selective for L- than D-lactate[84]. We found that L-lactate was progressively consumed by WT *S. aureus* biofilm, whereas D-lactate persisted at much higher levels, since it is not utilized by *S. aureus* as a carbon source[85,86]. In addition, D-lactate was significantly increased in the synovial fluid of patients with PJI compared to aseptic cases, in agreement with a recent study[87]. Therefore, although MCT-1 has a higher Km for D-lactate, local concentrations in the biofilm milieu exceed that of L-lactate, making D-lactate uptake feasible. Our finding that D-lactate levels were elevated irrespective of the causative pathogen in human PJI demonstrates the broader implications of lactate on modulating host immunity during biofilm infection caused by other bacterial species.

The infection-associated epigenetic dysregulation[88] by *S. aureus* lactate shown in this study likely culminates from a variety of interrelated factors, including chronic interactions between *S. aureus* and environmental signals and co-adaptation of host leukocytes with *S. aureus* during persistent infection. This is plausible when considering the fact that the lactate-dependent phenotypes on leukocyte activation and bacterial burden were most evident at later stages of infection (i.e. days 14 and 28), in agreement with the delayed kinetics of IL-10 action in the mouse PJI model that manifest at day 14 post-infection[16]. Of note, some IL-10 production was still evident *in vivo* in the absence of *S. aureus* lactate. This was not attributed to host lactate, since residual IL-10 levels were not affected after inhibiting host LDH. Therefore, lactate-independent mechanisms exist for inducing maximal IL-10 production, which is not unexpected given the large number of *S. aureus* virulence determinants[54,89]. Collectively, these findings identify *S. aureus* biofilm-derived lactate as a metabolic virulence factor that augments IL-10 production in MDSCs and macrophages by inhibiting HDAC11. This serves to attenuate leukocyte pro-inflammatory activity, representing one mechanism to account for biofilm persistence.

MATERIALS AND METHODS

Mice.

C57BL/6NCrl (RRID:IMSR_CRL:27), IL-10 KO (RRID:IMSR_JAX:002251), and HDAC11 KO mice (RRID:IMSR_TAC:6978)[90] were used for experiments. C57BL/6NCrl and IL-10 KO animals were bred in house at the University of Nebraska Medical Center (UNMC) and mice of the same sex were randomized into standard density cages upon weaning (n= 5 animals per cage). Mice were housed in a restricted-access BSL2 room equipped with ventilated microisolator cages and maintained at 21°C under a 12 h light:12 h

dark cycle with ad libitum access to water (Hydropac™; Lab Products, Seaford, DE) and Teklad rodent chow (Harlan, Indianapolis, IN) with Nestlets provided for enrichment. This study was conducted in strict accordance with the recommendations in the *Guide for the Care and Use of Laboratory Animals* of the National Institutes of Health. The animal use protocol was approved by the UNMC Institutional Animal Care and Use Committee (#18-013-03).

S. aureus *strains.*

The Nebraska Transposon Mutant Library (NTML) was constructed in LAC JE2[28]. Δ*ddh*, Δ*ldh1*, Δ*ldh2*, and Δ*lctP1* Tn mutants were moved to the USA300 LAC 13c background by transduction with bacteriophage φ11[28] (Extended Data 1a). Lactate double (Δ*ldh1/ldh2*) and triple (Δ*ddh/ldh1/ldh*) mutants were constructed from each single Tn mutant after switching antibiotic resistance cassettes associated with the Tn mutant. Transposon insertions were confirmed by PCR using chromosomal primers flanking the gene containing the Tn insertion. All *S. aureus* strains were transduced with a GFP plasmid (pCM13)[91] and imaged using a Zeiss 710 META laser scanning microscope (Carl Zeiss) after 4 days of biofilm growth to evaluate biofilm structure.

S. aureus *biofilm growth.*

Single colonies of WT, Δ*ddh*, Δ*ldh1/ldh2*, and Δ*ddh/ldh1/ldh2* were inoculated into 5mL of RPMI-1640 supplemented with 10% FBS (Cat. #SH30079.02HI; HyClone), 1% HEPES (Cat. #SH40003.01; Hyclone) and 1% L-glutamine (Cat. #25–005-CL; Corning) and grown overnight at 37°C, with shaking (250 rpm). Overnight cultures were inoculated at a 1:100 dilution in 96-well plates pre-coated with 20% human plasma (generously provided by Dr. Scott Koepsell, UNMC) as previously described[92]. Biofilms were grown under static conditions at 37°C in room air. After every 24 h of growth, approximately 35% of the medium was removed and replaced with fresh medium to avoid disturbing biofilm structure. Lactate levels in static biofilms ranged from 200–1500 μM, which is less than the mM concentrations reported during planktonic growth[29,46]. This was attributed, in part, to lactate consumption, as revealed by the progressive reduction in L-lactate over a 24 h period in WT biofilm (Extended Data 6a and b), since it can be utilized by *S. aureus* to form pyruvate under glucose deplete conditions[46].

Generation of bone marrow-derived MDSCs and macrophages for *in vitro* biofilm co-culture experiments.

MDSCs and macrophages were expanded from the bone marrow of WT, HDAC11 KO, TLR2 KO (RRID:IMSR_JAX:004650), or MyD88 KO (RRID:IMSR_JAX:009088) mice as previously described[16,93]. Briefly, $Ly6G^+$ MDSCs were purified using an anti-Ly6G MicroBead Kit (Cat. # 130-092-332; Miltenyi Biotec) after 4 days in culture, per the manufacturer's instructions. The resulting $Ly6G^+$population has been verified for Ly6C expression and is phenotypically and functionally similar to MDSCs infiltrating *S. aureus* implant-associated biofilm *in vivo*[16]. For macrophage cultures, FACS analysis revealed that > 95% of cells were macrophages based on CD11b and F4/80 staining after a 7 day culture period[93]. Bone marrow-derived MDSCs and macrophages (5×10^4) were added to 4 day-old *S. aureus* WT and lactate mutant biofilm for 2 h to assess IL-10 production. For metabolic

complementation experiments, lactate mutant biofilms were treated with sodium D- or L-lactate (both at 2.5 μM; Cat. #s 71716 and 71718, respectively; Sigma-Aldrich) at the time of MDSC or macrophage addition. The MCT1 inhibitors AZD3965 and 7ACC2 (both at 10 nM; Cat. #s 19912 and 1472624-85-3, respectively; Cayman Chemical Company) and HDAC6 inhibitors tubastatin A (15nM) and HDAC6i (36nM) (Cat. #s 15785 and 1259296-46-2, respectively; Cayman Chemical Company) were included at the time of MDSC or macrophage addition to biofilm.

Gentamicin protection assay.

Bone marrow-derived macrophages were prepared as described above. Macrophages were seeded in a 96-well plate at 5×10^4 cells/well and incubated with WT, Δ*ddh*, Δ*ldh1/ldh2*, or Δ*ddh/ldh1/ldh2 S. aureus* strains at a MOI of 10:1 or 50:1 for 45 min at 37°C, 5% CO_2. Plates were washed and incubated for another 30 min in medium containing 100 μg/mL gentamicin (Cat. #G1264, Millipore Sigma) to kill residual extracellular bacteria, whereupon cells were washed and medium containing 1 μg/mL gentamicin was added. Intracellular bacterial loads were determined at 0, 2, 4, 6 and 24 h following low dose gentamicin treatment by lysing macrophages with sterile water and plating on blood agar. This approach confirmed that the reduced survival of Δ*ddh*, Δ*ldh1/ldh2*, or Δ*ddh/ldh1/ldh2 in vivo* was not due to enhanced sensitivity to immune-mediated clearance, since macrophage bactericidal activity was similar for all mutants (Supplementary Figure 3).

D- and L-lactate and IL-10 quantification.

D- and L-lactate concentrations in supernatants from *S. aureus* WT and lactate mutant biofilm *in vitro,* mouse implant-associated tissue homogenates, and human synovial fluid were determined using D- and L-Lactate colorimetric assays according to the manufacturer's instructions (Cat. #s K667–100 and K607–100, respectively; BioVision). Murine IL-10 levels in supernatants from MDSC- or macrophage-biofilm co-cultures and tissue homogenates were quantified using a Mouse Inflammation Cytometric Bead Array (CBA; Cat #552364, BD Biosciences) or sandwich ELISA (Mouse DuoSet; Cat. #DY417–05, R&D Systems). IL-10 in human synovial fluid samples and human monocyte-derived macrophages was measured by ELISA (Cat. #430604, BioLegend).

Mouse model of *S. aureus* orthopaedic biofilm infection.

To model infectious complications in patients following orthopaedic device placement, a mouse model of *S. aureus* PJI was used as previously described[14–16,18,94–97]. This model reflects biofilm growth as demonstrated by scanning electron microscopy and H&E staining[14,15,18,95,96]. In addition, immunophenotyping of patients with PJI, many of which were diagnosed with *S. aureus*, has identified similar leukocyte infiltrates as observed in the mouse model[15,83], supporting its translational utility. The sample size for *in vivo* experiments was based on prior work from our laboratory[14–16,93,94,98], which was shown to provide statistically significant findings. Both male and female mice were used for these studies between the ages of 8–10 weeks and the study was not blinded to strain or treatment status. Mice were anesthetized with ketamine/xylazine and a medial incision was made through the quadriceps. Following lateral displacement of the patellar tendon, a burr hole was created in the intercondylar notch with a 26-gauge needle, whereupon an orthopaedic-

grade K-wire (0.6 mm diameter, nitinol [nickel-titanium]; Custom Wire Technologies) was inserted. A total of 1,000 CFU of *S. aureus* WT or lactate mutant strains were inoculated at the implant tip. For co-infection experiments, mice were infected with a 1:1 ratio of WT and Δ*ddh/ldh1/ldh2 S. aureus* (each at 1,000 CFU) and strains were differentiated based on antibiotic resistance profiles. Buprenex was administered for pain relief immediately after surgery and 24 h later, at which point mice exhibited normal ambulation and no discernable pain behaviors. For HDACi experiments, mice received daily i.p. injections of the pan-HDACi trichostatin A (0.5 mg/kg; Cat. #89730; Cayman Chemical) or the HDAC6i tubastatin A (0.5 mg/kg; Cat. #15785; Cayman Chemical Company) beginning on the day of infection. To inhibit host LDH, mice received daily i.p. injections of sodium oxamate (500 mg/kg; Cat. #19057; Cayman Chemical) dissolved in 0.5% Hydroxypropyl Methylcellulose beginning one day prior to infection.

Quantification of leukocyte infiltrates and biofilm burden.

The soft tissue surrounding the infected knee joint as well as the femur was collected after removing the skin, weighed, and homogenized, as previously described[15]. Serial, 10-fold dilutions of tissue and femur homogenates were plated on TSA with 5% sheep blood (Cat #R01202; Remel Products), with titers expressed as CFU per gram of tissue. Remaining homogenates were centrifuged (20,000x*g*, 20 min) and frozen at −80°C until analysis.

To quantify leukocyte infiltrates in the implant-associated soft tissue of mice infected with WT *S. aureus* or lactate mutants, homogenized tissues were filtered and red blood cells (RBCs) removed from the single cell suspension using RBC Lysis Buffer (Cat. #420301; BioLegend). After lysis, leukocytes were incubated with Fc Block (TruStain FcX, Cat. #101320; BioLegend) and stained with CD45-PacBlue (RRID:AB_493535), Ly6G-PE (RRID:AB_1186099), F4/80-PE-Cy7 (RRID:AB_893478), and CD11b-FITC (RRID:AB_312789) (all from BioLegend) or Ly6C-PerCP-Cy5.5 (RRID:AB_1727558, BD Pharmingen). Dead cells were excluded from analysis using a Live/Dead Fixable Blue Dead Cell Stain Kit (Cat. #L23105; Invitrogen) and analysis was performed using BD FACSDiva software (RRID:SCR_001456) as previously described[94] using the gating strategy presented in Extended Data 10. To monitor leukocyte intracellular pH, MDSCs and macrophages were labeled with BCECF-AM (10 μM; Cat. #B1150, ThermoFisher) prior to co-culture with WT or Δ*ddh/ldh1/ldh2* biofilm for 2 h, whereupon intracellular pH was determined by flow cytometry based on a standard curve of known pH.

Quantitative real-time reverse transcription PCR (RT-qPCR).

$Ly6G^{-}Ly6C^{+}F4/80^{-}$ monocytes and $CD11b^{high}Ly6G^{+}Ly6C^{+}$ MDSCs were purified from mice infected with WT *S. aureus* or Δ*ddh/ldh1/ldh2* by FACS, whereupon total RNA was immediately isolated using a Micro RNeasy kit (Cat. #74004; Qiagen). RT-qPCR was performed using TaqMan primer/probe mixes (ThermoScientific) for arginase-1 (Arg-1; Cat. #Mm00475988_m1), TNF-α (Cat. #Mm00443258_m1), IL-10 (Cat. #Mm00439616_m1), and glyceraldehyde-3-phosphate dehydrogenase (GAPDH; Cat. #Mm99999915_g1). Gene expression levels were normalized to GAPDH and are presented as the fold-induction ($2^{-\Delta\Delta Ct}$) for leukocytes from Δ*ddh/ldh1ldh1*-infected mice relative to WT.

In some experiments, gene expression was analyzed in FACS purified Ly6G^{-}Ly6C^{+}F4/80^{-} monocytes and CD11b^{high}Ly6G^{+}Ly6C^{+} MDSCs by Nanostring. RNA samples (25–50 ng each) were hybridized to the nCounter® Mouse PanCancer IO 360™ Panel Reporter CodeSet and Capture CodeSets (Cat. #115000260; NanoString Technologies) overnight for 16 h at 65°C per the manufacturer's instructions. Following hybridization, samples were loaded on the detection cartridge using the nCounter MAX/FLEX System at the High Sensitivity setting and processed on the nCounter Digital Analyzer for a counting time of 5 h. Initial sample analysis was performed using the nSolver™ 4.0 Analysis Software (RRID:SCR_003420). Quality metrics were reviewed and the results were normalized to the housekeeping genes provided by Nanostring. Following normalization, data were analyzed to determine fold-changes, where differentially expressed genes were identified based on a p-value < 0.05.

HDAC activity in cells recovered from *S. aureus* orthopaedic implant biofilm infection.

Implant-associated tissues from mice infected with WT or Δ*ddh/ldh1/ldh2 S. aureus* were collected at day 14 post-infection and dissociated as described above. Following RBC lysis, cells were plated at 1×10^{5} cells/well in a flat-bottom 96-well plate. HDAC activity was measured using a FLUOR DE LYS® HDAC fluorometric activity assay kit (Cat. #BML-AK503–0001; Enzo Life Sciences). The relative amount of H3Ac in lysates of leukocytes from WT or Δ*ddh/ldh1/ldh2*-infected mice was quantified using a Pathscan ELISA kit (Cat. #7232C; Cell Signaling Technology), according to the manufacturer's instructions.

Cell-free HDAC activity assay.

Human recombinant HDAC6 and HDAC11 were purchased in their active forms from Enzo Life Sciences (Cat #BML-SE508–0050 and BML-SE-560–0050, respectively) and incubated with conditioned medium from WT or Δ*ddh/ldh1/ldh2 S. aureus* biofilm for 30 min, whereupon enzymatic activity was quantified using a FLUOR DE LYS® HDAC fluorometric activity assay kit (Cat. #BML-AK503–0001; Enzo Life Sciences).

Chromatin immunoprecipitation sequencing (ChIP-seq), ChIP-PCR, and scRNA-seq.

ChIP-seq was performed on CD11b^{high}Ly6G^{+}Ly6C^{+} MDSCs isolated from mice infected with WT or Δ*ddh/ldh1/ldh2 S. aureus* at day 14 post-infection. For each sample, chromatin immunoprecipitation DNA was acquired using a histone pan-H3Ac antibody (RRID: AB_2793714; Active Motif) and a Zymo-Spin ChIP kit (Cat. #D5209; Zymo Research) according to the manufacturer's instructions. The captured and purified DNA was prepared for high-throughput sequencing using the NEBNext Ultra II DNA Library Prep kit for Illumina (Cat. #E7645S; New England Biolabs). The resulting indexed libraries were sequenced by the UNMC DNA Sequencing Core Facility using an Illumina NextSeq 500 Genome Analyzer (RRID:SCR_014983). Initial raw sequence files were adaptor trimmed using Trim Galore software (RRID:SCR_016946) and the resulting fastq files were aligned to the mouse genome using the sequence aligner Bowtie2 (version 2.2.3)[99]. The software package Picard routine MarkDuplicates (http://broadinstitute.github.io/picard/; RRID:SCR_006525) was used to remove sequence duplications. A sequencing count of 49.7 million was acquired using SAMTOOLS (http://samtools.sourceforge.net/; RRID:SCR_002105) for each sample. For peak calling of ChIP-enriched regions, THOR

peak caller[100] software (RRID:SCR_001400) of each ChIP to corresponding input DNA sample was used, which utilizes a pipeline consisting of estimation of fragment size, DNA mappability, GC-content normalization, correction of signals with input DNA, and signal normalization. Density estimates from the Hidden Markov Model-based approach was employed coupled to negative binomial distribution, and an exact statistical test was run[101] to assign a *p*-value to each ChIP-enriched region. Significant ChIP-enriched regions with a distance less than the mean of all estimated fragment sizes were merged and *p*-values were corrected using the Benjamini and Hochberg method of controlling for False Discovery Rate (FDR). Using this approach, ChIP-enriched binding regions were determined based on a FDR adjusted *p*-value (q-value) < 0.05. BigWig files were generated using the Deeptools bamCoverage routine (https://deeptools.readthedocs.io/en/develop/; RRID:SCR_016366). Alignment of significant peaks to gene-specific regions was accomplished using the BEDTools routine intersect (https://bedtools.readthedocs.io/en/latest/; RRID:SCR_006646).

For ChIP-qPCR, specific primers (Supplementary Table 2) were designed for two regions that indicated a significant change in H3Ac abundance associated with *IL-10* and a region designated as an *IL-10* STAT3 binding site[65]. Gradient annealing temperature q-PCR was performed for each primer set. The input DNA pulled from ChIP was diluted 10-fold with 10 μL Bio-Rad iTaq Universal SYBR Supermix (Cat. #1725120), 2.5 μL each forward/reverse primers (0.625 μM final concentration), and 4 μL H_2O. q-PCR was performed using a Bio-Rad CFX Real-Time System with the following program: 1 min at 95°C; 45 cycles of 95°C for 15 s, 60°C for 20 s, and 72°C for 20 s. Percent Input Method was calculated as previously described[102] and the delta-delta method[103] was performed using two calibrator primer sets, namely 1) Negative Mouse Control Primer Set 1 (Cat #71011; Active Motif) that interrogates a gene desert region on chromosome 6; and 2) Mouse Positive Control Primer Set Actb-2 (Cat. #71017; Active Motif) that interrogates a region in the Actb promoter. ChIP-Seq data was validated in FACS-purified MDSCs collected at day 14 post-infection by RT-qPCR for the following genes; insulin-like growth factor 1 (Igf1; Cat. #Mm00439560_m1), granzyme C (Gzmc; Cat. #Mm01313651_m1), macrophage galactose N-acetyl-galactosamine specific lectin 2 (Mgl2; Cat. #Mm00460844_m1), resistin-like gamma (Retnlg, Cat. #Mm00731489_s1), interferon-beta (IFN-b1; Cat. #Mm00439546_s1), and MCT1 (Slc16a1; Cat. #Mm01306379_m1). Gene expression levels were normalized to GAPDH (Cat #Mm99999915_g1) and are presented as the fold-induction ($2^{-\Delta\Delta Ct}$) for leukocytes from Δ*ddh/ldh1ldh1*-infected mice relative to WT.

For single cell RNA-sequencing (scRNA-seq), live, $CD45^+$ leukocytes from tissues surrounding WT or Δ*ddh/ldh1/ldh2*-infected implants were isolated by FACS at day 14 post-infection and prepared for sequencing in the UNMC DNA Sequencing Core Facility. Briefly, sorted leukocytes were evaluated by light microscopy to determine concentration, percent viability, and to assess potential debris present in the suspension. Cells were loaded onto a 10X Genomics instrument and single cells were captured, lysed, RNA reverse transcribed, and RNA barcoded using a Chromium Single Cell 3' Reagent Kit v3 (Cat. #PN-1000075; 10X Genomics), according to the manufacturer's instructions. Illumina compatible cDNA libraries were created and quantified by qPCR using the KAPA Library Quant Kit (Illumina) (Cat. #KK4824; KAPA Biosystems) and were loaded at a concentration of 1.3 pM on an Illumina NextSeq550 instrument. Samples were sequenced following the parameters

suggested by 10X Genomics to an average depth of approximately 50,000 reads per cell. Expression differences between leukocytes from WT and Δ*ddh/ldh1/ldh2*-infected mice were performed using the 10X Genomics R2 read fastq files and analyzed as single end bulk RNA-seq analysis based on the following steps. Adaptor sequences and low quality (Phred score: 20) ends were trimmed from sequences using the Trim Galore software package (http://www.bioinformatics.babraham.ac.uk/projects/trim_galore/) and the resulting fastq files were aligned to the mouse genome (GRCm38/mm10) using the software TopHat (v2.0.8) (http://ccb.jhu.edu/software/tophat/index/shtml/; RRID:SCR_013035). The software Cufflinks (v2.1.1) (http://cole-trapnell-lab.github.io/cufflinks/; RRID:SCR_014597) was used to estimate the expression values and Cuffdiff (V2.1.1; RRID:SCR_001647) was used to determine differential expression. Alignment of significant H3Ac peaks to gene-promoter regions was accomplished using the BEDTools routine intersect (https://bedtools.readthedocs.io/en/latest/). Excel logic formulas were used to select genes that were increased or decreased in both expression and H3Ac. The complete ChIP-Seq and scRNA-seq datasets have been deposited in the GEO repository (accession number GSE135496).

Human monocyte-derived macrophages and patient samples.

Human monocytes were obtained from healthy human donors by the UNMC Elutriation Core Facility by countercurrent centrifugal elutriation, in full compliance and approval of the Institutional Review Board (IRB). Cells were cultured at 1×10^6 cells/mL in RPMI-1640 supplemented with recombinant human M-CSF (100ng/mL; Cat. #574802; BioLegend), 10% human serum (Cat. #H4522; Millipore Sigma) and penicillin/streptomycin/fungizone (Cat. #30–004-CI; Corning) for 7 days. For macrophage treatment with clarified biofilm supernatants, conditioned medium was collected from mature *S. aureus* WT and Δ*ddh/ldh1/ldh2* biofilm and centrifuged at 4,000x*g* for 10 min, followed by filtration (0.22 μM) and ultracentrifugation at 100,000x*g* for 2 h at 4°C. A total of 1×10^6 human monocyte-derived macrophages were treated with a 1:10 dilution of clarified biofilm supernatant from WT or Δ*ddh/ldh1/ldh2* biofilm for 2 h ± the HDAC6i tubastatin A (15 nM; Cat. #15785; Cayman Chemical Company). Clarified biofilm supernatants were used for these experiments due to the rapid death of human cells during *S. aureus* biofilm co-culture.

Informed consent was obtained from patients undergoing primary or revision total knee or total hip arthroplasty for infectious or aseptic complications during their pre-surgical visit, following prior approval by the UNMC IRB (#177–14-FB and 657–13-EP). Subjects included both males and females between 43–81 years of age. Synovial fluid was collected intraoperatively for D- and L-lactate assays as described above and organisms associated with PJIs were identified by the Clinical Microbiology Laboratory at UNMC. Samples that were negative for bacterial growth using standard protocols were classified as aseptic. In terms of the relationship between bacterial lactate and HDACi, although a prior report demonstrated that lactate inhibits HDACs at mM concentrations *in vitro*[36], which exceed the levels detected in human PJI, it is important to note that the synovial fluid samples in our study were collected at the time of surgery when patients were already undergoing antibiotic treatment. Therefore, these lactate measurements are likely an under-representation of levels in the infected joint prior to antibiotic treatment when the immune modulatory effects of bacterial-derived lactate would be operative.

Statistics.

Significant differences between experimental groups were determined by an unpaired two-tailed Student's *t*-test or a one-way ANOVA with Tukey's or Dunnett's multiple comparisons post-hoc test using GraphPad Prism version 6.04 (LaJolla, CA; RRID:SCR_002798). For all analyses, $p < 0.05$ was considered statistically significant.

Extended Data

a

Bacterial Strain or plasmid	Relevant phenotype	Source
S. aureus LAC13c	Wild-type USA300 isolate	(10)
pCM13	P_{sarA}::gfp_{ermR}	(91)
Δ*ddh*	*S. aureus* LAC13c *ddh*::$\Phi N\Sigma_{ermR}$	This study
Δ*ldh1*	*S. aureus* LAC13c *ldh1*::$\Phi N\Sigma_{markerless}$	This study
Δ*ldh2*	*S. aureus* LAC13c *ldh2*::$\Phi N\Sigma_{ermR}$	This study
Δ*ldh1/ldh2*	*S. aureus* LAC13c *ldh1*::$\Phi N\Sigma_{ermR}$ *ldh2*::$\Phi N\Sigma_{spcR}$	This study
Δ*ddh/ldh1/ldh2*	*S. aureus* LAC13c *ddh*::$\Phi N\Sigma_{kanR}$ *ldh1*::$\Phi N\Sigma_{ermR}$ *ldh2*::$\Phi N\Sigma_{spcR}$	This study
ΔlctP1	*S. aureus* LAC13c *lctP*::$\Phi N\Sigma_{ermR}$	This study

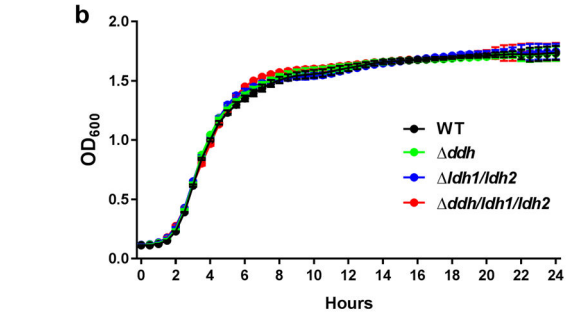

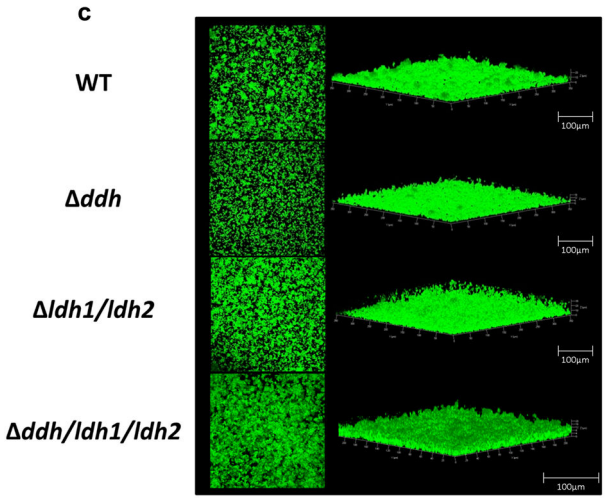

Extended Data Fig. 1. *S. aureus* lactate mutants do not display growth defects in liquid broth or biofilm *in vitro*.

(**a**) *S. aureus* strains used in this study. (**b**) The growth rate of *S. aureus* WT, Δ*ddh*, Δ*ldh1/ldh2*, and Δ*ddh/ldh1/ldh2* was determined in brain-heart infusion broth over a 24 h period with constant agitation using a TECAN (7 biological replicates/strain). (**c**) Strains were transduced with a *sarA*-GFP plasmid and grown for 4 days under static growth conditions in

RPMI-1640 supplemented with 10% FBS, whereupon biofilm formation was visualized by confocal microscopy. Results are representative of two independent experiments, each with 4 biological replicates. Scale bars, 100 μm.

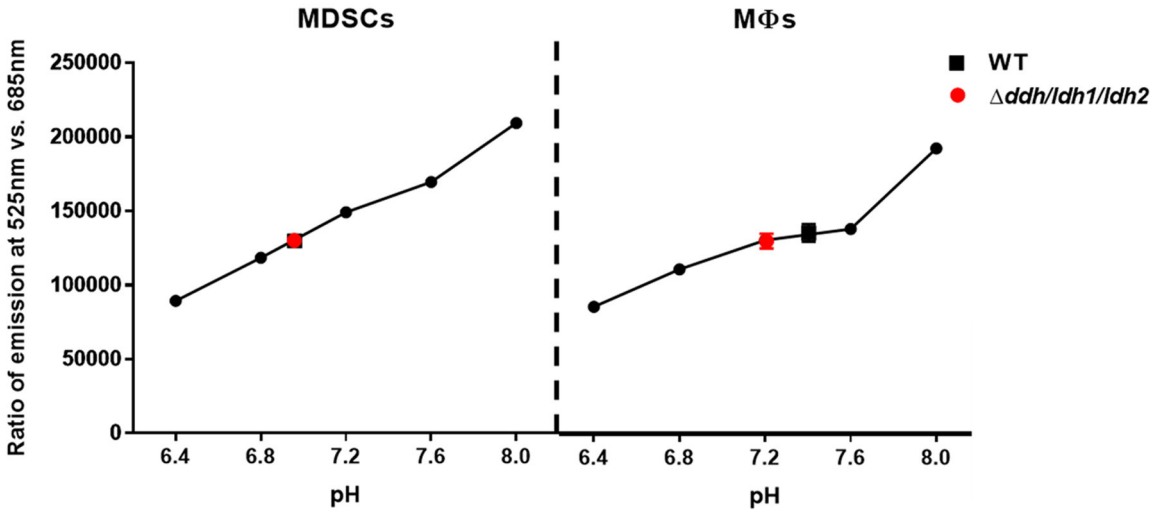

Extended Data Fig. 2. Intracellular pH of MDSCs and macrophages is not dramatically altered by *S. aureus*-derived lactate during biofilm co-culture.

MDSCs or macrophages were labeled with BCECF-AM (10 μM) prior to co-culture with WT (n=4 biological replicates/group) or Δ*ddh/ldh1/ldh2* (n=4 and 3 biological replicates for MDSCs and macrophages, respectively) biofilm for 2 h, whereupon intracellular pH was determined by flow cytometry based on a standard curve of known pH. Results shown are from one experiment.

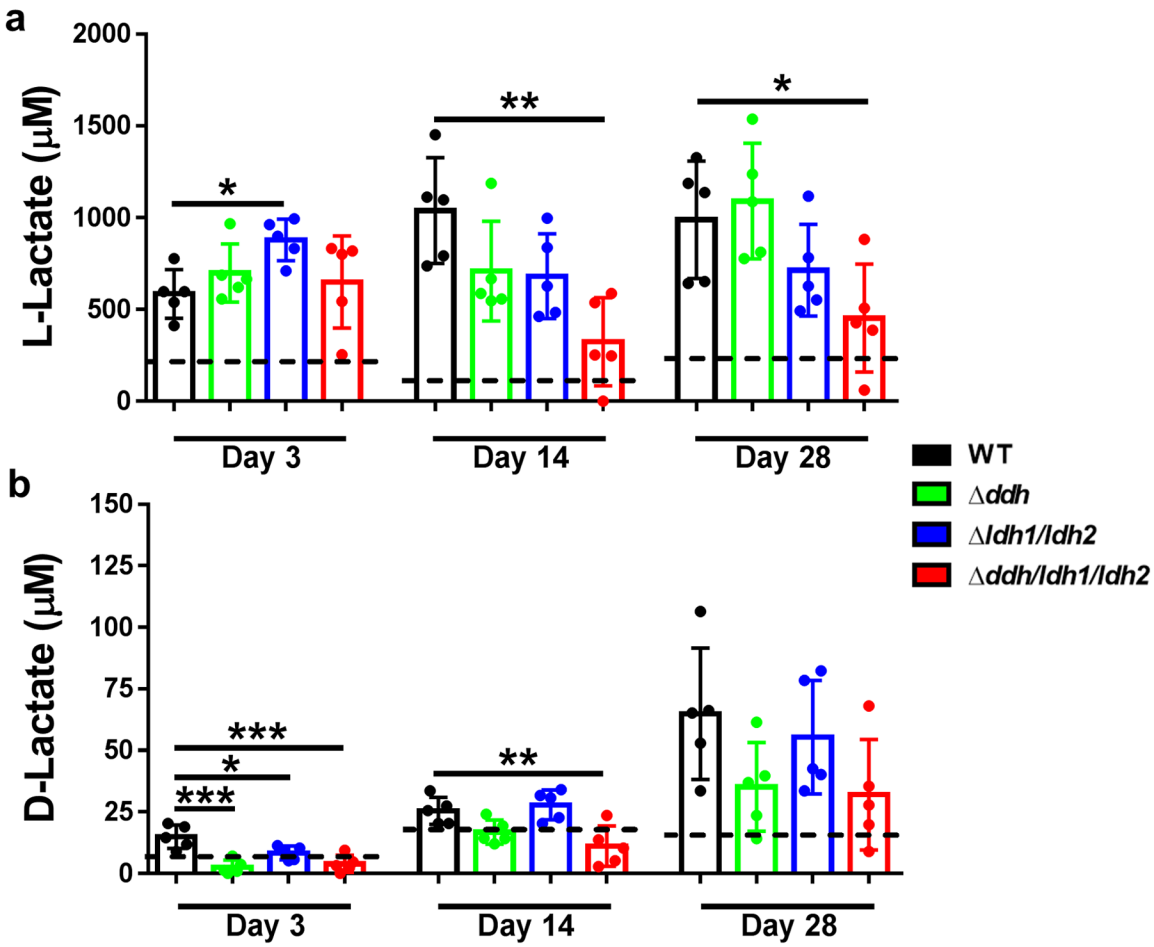

Extended Data Fig. 3. D- and L-lactate production during *S. aureus* orthopaedic infection.

(**a**) L- and (**b**) D-lactate were quantified in the implant-associated tissue of mice infected with WT, Δ*ddh*, Δ*ldh1/ldh2*, or Δ*ddh/ldh1/ldh2* at days 3, 14, and 28 post-infection (mean ± SD; n=5/group). The dashed line represents background in the assay as determined with tissues collected from animals receiving sterile implants at the same time points (n=5 at days 3 and 28 and n=4 at day 14). Results are representative of three independent experiments. *, $p < 0.05$; **, $p < 0.01$; ***, $p < 0.001$; One-way ANOVA.

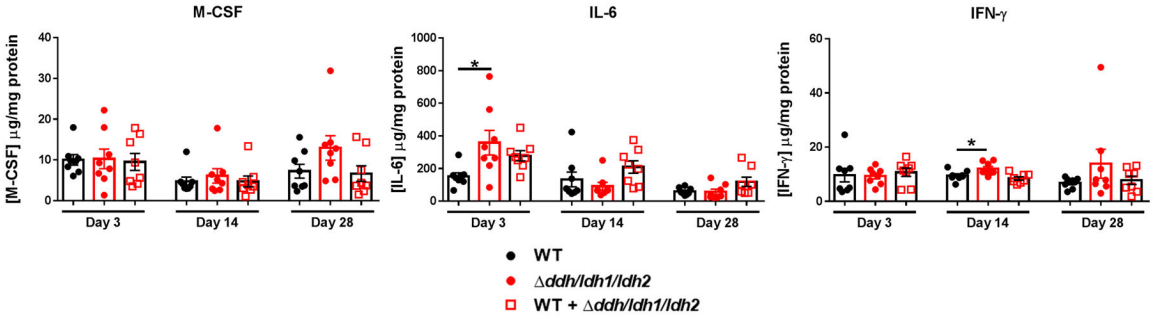

Extended Data Fig. 4. The expression of select inflammatory mediators is independent of bacterial burden during *S. aureus* orthopaedic infection.

Cytokine levels were quantified in implant-associated tissue of mice infected with WT, Δ*ddh/ldh1/ldh2*, or a 1:1 ratio of WT and Δ*ddh/ldh1/ldh2* at day 28 post-infection. Results are combined from two independent experiments (mean ± SD; n= 8/group). *, $p < 0.05$; One-way ANOVA.

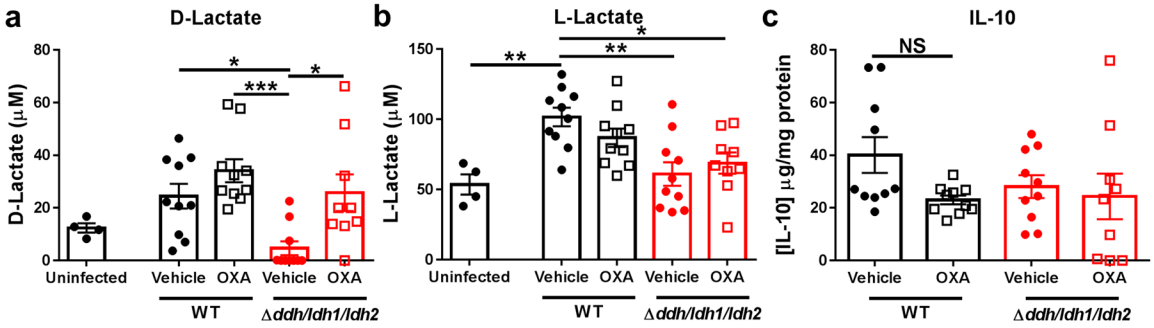

Extended Data Fig. 5. IL-10 production during *S. aureus* orthopaedic infection is not influenced by host lactate.

Mice received daily i.p. injections of sodium oxamate (500 mg/kg/day) dissolved in 0.5% Hydroxypropyl Methylcellulose or vehicle (0.5% Hydroxypropyl Methylcellulose) beginning one day prior to infection with *S. aureus* WT (n=10/group) or Δ*ddh/ldh1/ldh2* (n=10 or 9 for vehicle and oxamate, respectively). Mice were sacrificed at day 14 post-infection to quantify (**a**) D-lactate, (**b**) L-lactate, and (**c**) IL-10 in implant-associated tissue. Results are combined from two independent experiments (mean ± SD). D- and L-lactate measurements are also reported at day 14 for mice that received sterile implants (n=4/group). *, $p < 0.05$; **, $p < 0.01$; ***, $p < 0.001$; One-way ANOVA. NS, not significant.

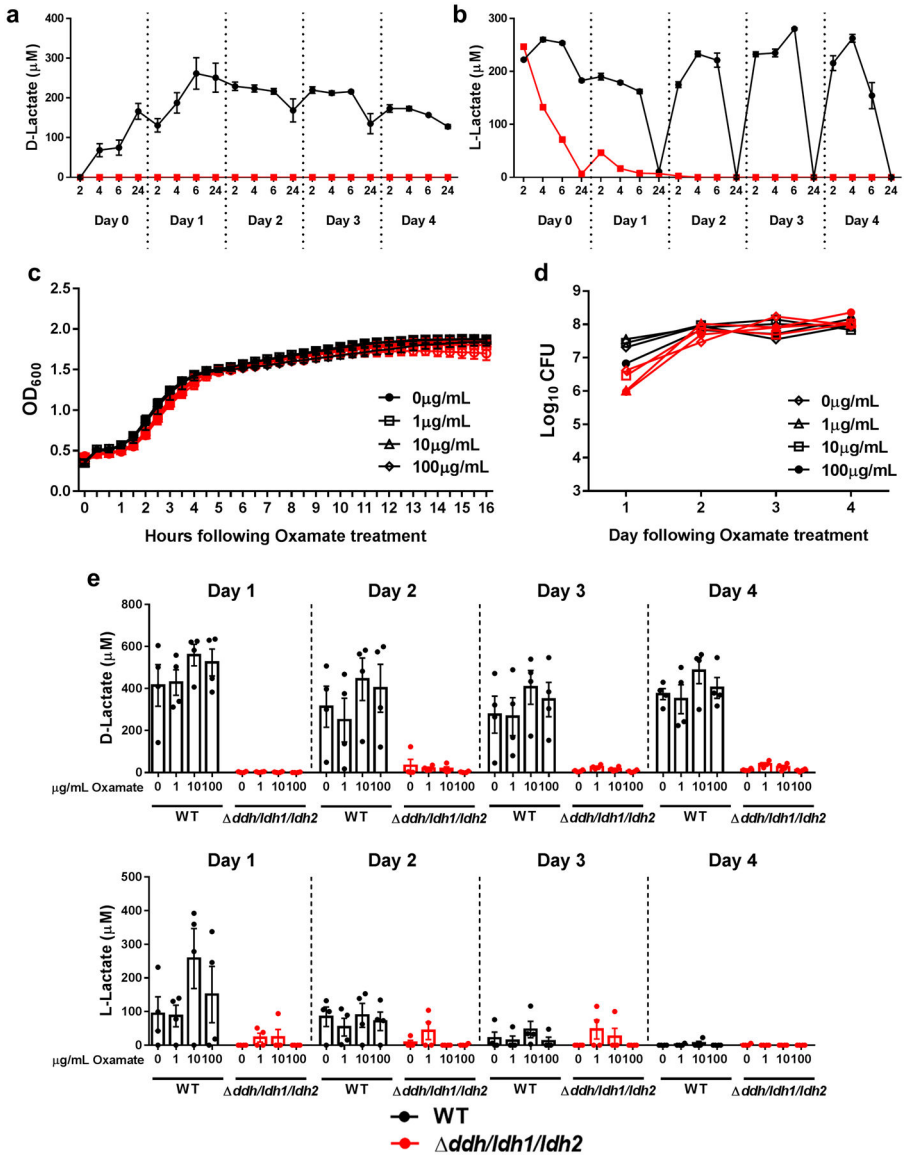

Extended Data Fig. 6. Sodium oxamate does not affect *S. aureus* growth or lactate production.

(**a**) D- and (**b**) L-lactate were quantified in *S. aureus* WT and Δ*ddh/ldh1/ldh2* biofilm in 96-well plates under static growth conditions in RPMI-1640 supplemented with 10% FBS over a 4 d period. The dotted lines represent daily medium changes. Results are from one experiment with 5 biological replicates. *S. aureus* was exposed to various concentrations of sodium oxamate during (**c**) growth in liquid broth (brain-heart infusion) beginning at time 0 (n=6 biological replicates/group) or (**d**) throughout the 4-day biofilm maturation period (n=5 biological replicates/group). Biofilm cultures were replenished daily with fresh medium (RPMI-1640 + 10% FBS) containing sodium oxamate. Results are presented as (**c**) OD_{600} or (**d**) Log_{10} colony forming units (CFU) per well. (**e**) Quantification of D- and L-lactate from biofilms throughout the 4-day growth period, where the dotted lines represent daily medium changes (n=4 biological replicates/group). All results are reported as mean ± SD.

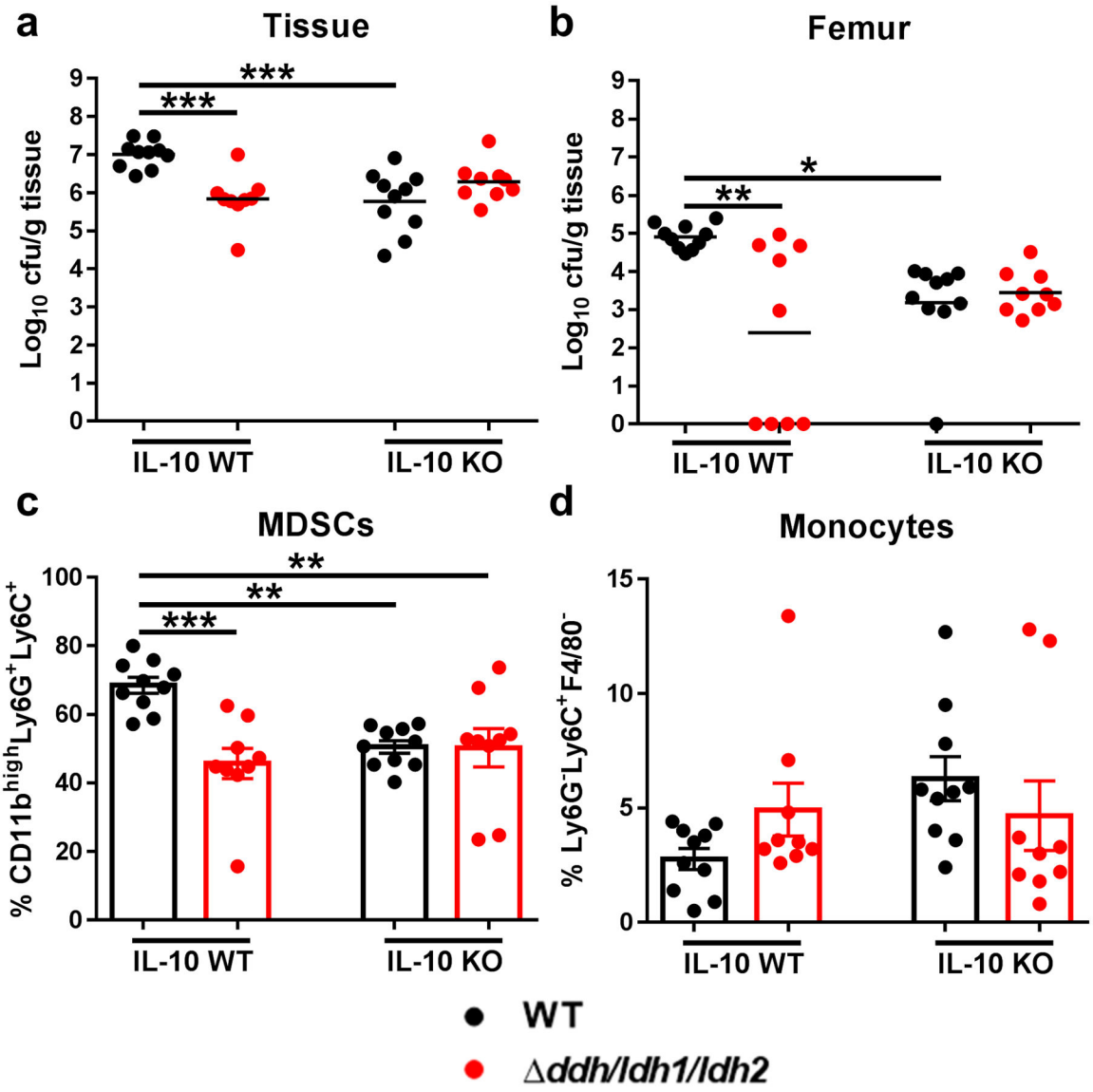

Extended Data Fig. 7. Effects of *S. aureus* lactate on orthopaedic implant biofilm infection are IL-10-dependent.

WT and IL-10 KO mice were infected with WT (n=10) or Δ*ddh/ldh1/ldh2* (n=9) *S. aureus*, whereupon bacterial burden in (**a**) implant-associated tissue and (**b**) femur as well as (**c**) MDSC and (**d**) monocyte infiltrates were assessed at day 14 post-infection. Results represent the mean ± SEM of two independent experiments. *, $p < 0.05$; **, $p < 0.01$; ***, $p < 0.001$; One-way ANOVA.

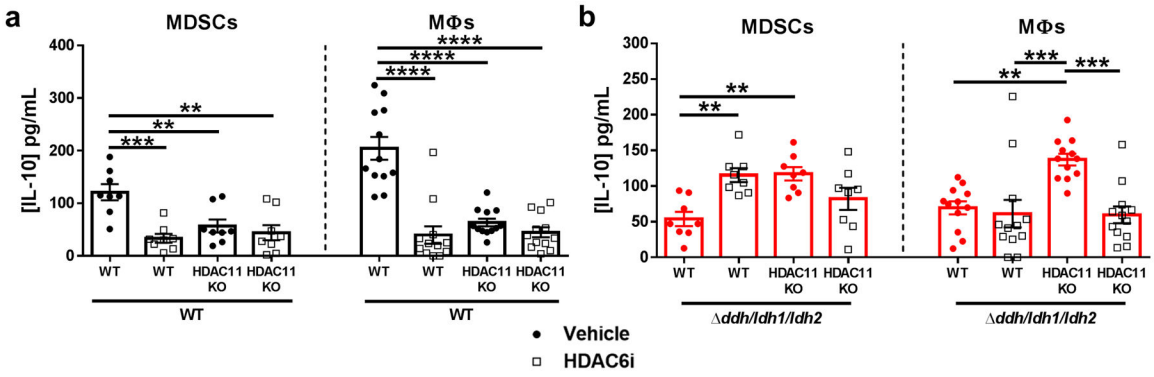

Extended Data Fig. 8. *S. aureus*-derived lactate inhibits the negative regulator HDAC11 to augment leukocyte IL-10 production in a HDAC6-dependent manner.

MDSCs and macrophages from WT or HDAC11 KO mice were co-cultured with (**a**) WT or (**b**) Δ*ddh/ldh1/ldh2* biofilm for 2h ± HDAC6i (36 nM). IL-10 production was measured by cytometric bead array. Results represent the mean ± SEM of two independent experiments (n=8 and 12 biological replicates for MDSCs and macrophages, respectively). **, $p < 0.01$; ***, $p < 0.001$; ****, $p < 0.0001$; One-way ANOVA. Values for untreated leukocytes are the same as those presented in Fig. 5a and b because both HDAC6i and tubastatin A were tested at the same time.

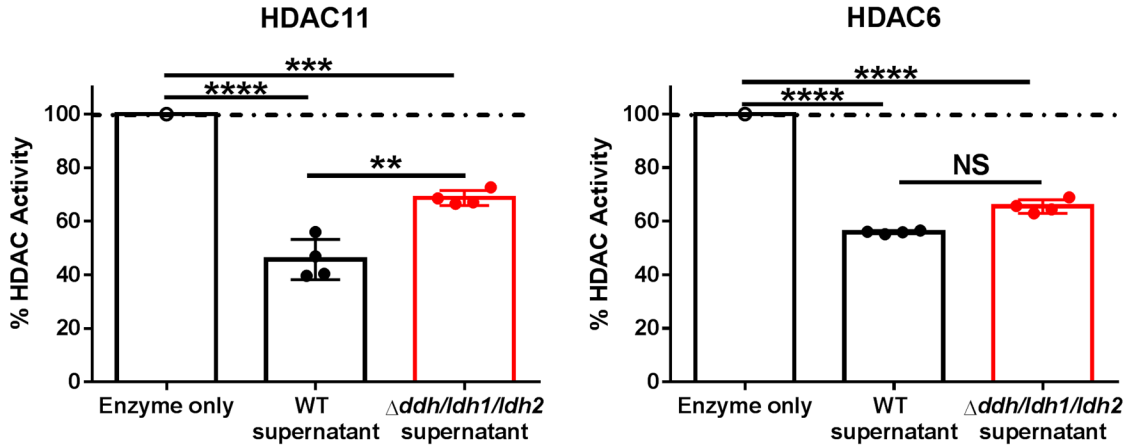

Extended Data Fig. 9. *S. aureus*-derived lactate preferentially inhibits HDAC11.

Purified active HDAC11 or HDAC6 were exposed to conditioned medium from WT or Δ*ddh/ldh1/ldh2* biofilm for 30 min, whereupon HDAC activity was determined using a fluorescent HDAC substrate (deAc-FdL). Results are from one experiment with 4 biological replicates and are expressed as the percent change in HDAC activity compared to purified enzyme. **, $p < 0.01$; ***, $p < 0.001$; ****, $p < 0.0001$; One-way ANOVA. NS, not significant.

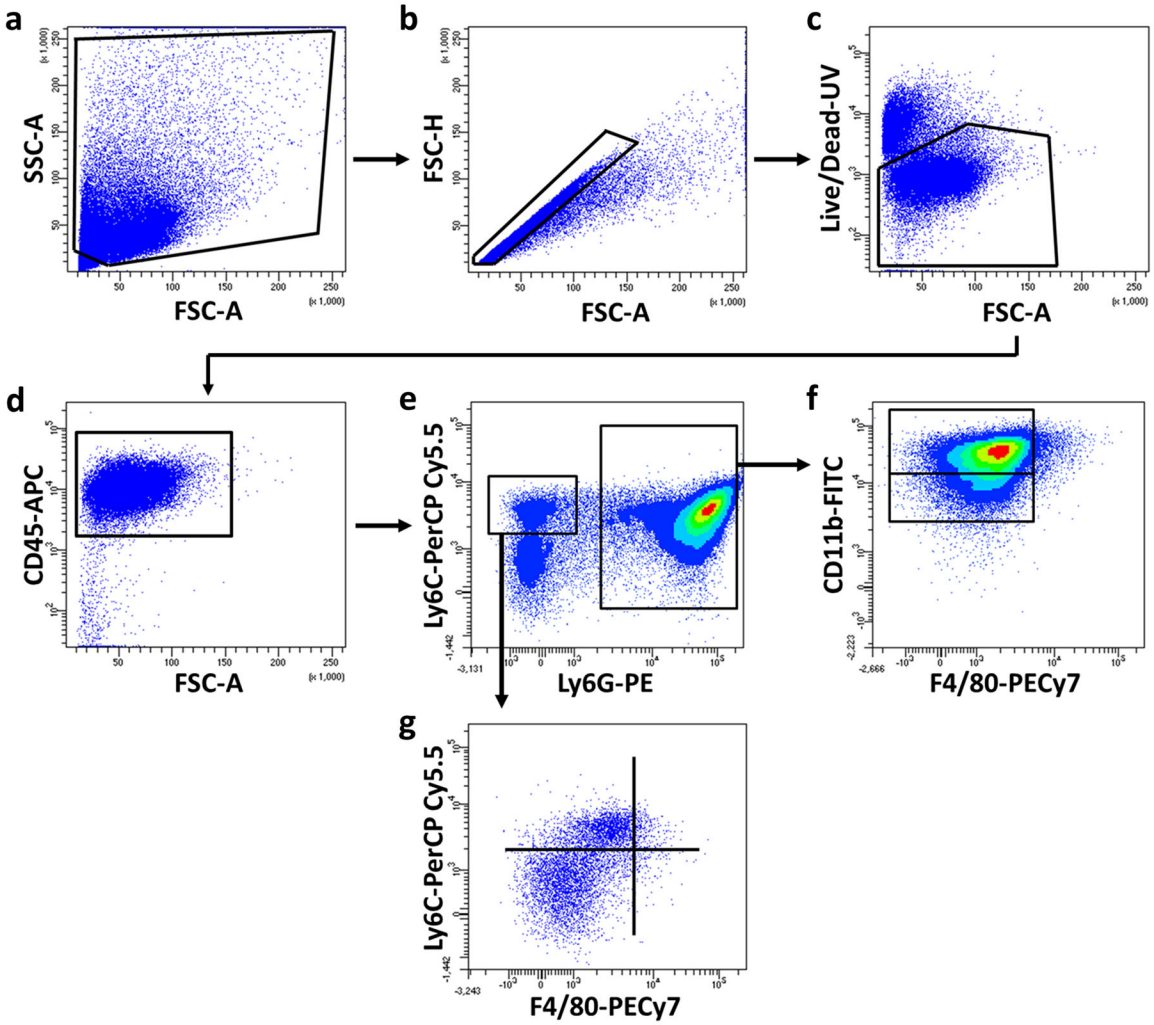

Extended Data Fig. 10. Gating strategy to quantitate leukocyte populations in *S. aureus* implant-associated soft tissue.

Single cells were gated from the (**a**) total events using (**b**) FSC-A vs. FSC-H, followed by (**c**) exclusion of dead cells. (**d**) Live, $CD45^+$ leukocytes were separated into (**e**) $Ly6G^+Ly6C^+$ vs. $Ly6G^-Ly6C^+$. (**f**) MDSC and neutrophil populations were identified based on CD11b expression, while (**g**) monocyte and macrophage populations were identified based on Ly6C and F4/80 expression, respectively.

Supplementary Material

Refer to Web version on PubMed Central for supplementary material.

ACKNOWLEDGEMENTS

This work was supported by the National Institutes of Health/National Institute of Allergy and Infectious Disease grant P01AI083211 (Project 4 to TK) and R01AI125588 to VCT. The authors thank Rachel Fallet for managing the mouse colony and Dr. Kari Nelson for editorial review of the manuscript. The UNMC DNA Sequencing Core receives partial support from the National Institute for General Medical Science (NIGMS; INBRE - P20GM103427-14 and COBRE - 1P30GM110768-01). Both the UNMC DNA Sequencing and Flow Cytometry Research Cores receive support from The Fred & Pamela Buffett Cancer Center Support Grant (P30CA036727).

REFERENCES

1. Percival SL, Suleman L, Vuotto C & Donelli G Healthcare-associated infections, medical devices and biofilms: risk, tolerance and control. J Med Microbiol 64, 323–334, doi:10.1099/jmm.0.000032 (2015). [PubMed: 25670813]
2. Pulido L, Ghanem E, Joshi A, Purtill JJ & Parvizi J Periprosthetic joint infection: the incidence, timing, and predisposing factors. Clin Orthop Relat Res 466, 1710–1715, doi:10.1007/s11999-008-0209-4 (2008). [PubMed: 18421542]
3. Arciola CR, Campoccia D & Montanaro L Implant infections: adhesion, biofilm formation and immune evasion. Nat Rev Microbiol 16, 397–409, doi:10.1038/s41579-018-0019-y (2018). [PubMed: 29720707]
4. Flemming HC et al. Biofilms: an emergent form of bacterial life. Nat Rev Microbiol 14, 563–575, doi:10.1038/nrmicro.2016.94 (2016). [PubMed: 27510863]
5. Balaban NQ et al. Definitions and guidelines for research on antibiotic persistence. Nat Rev Microbiol 17, 441–448, doi:10.1038/s41579-019-0196-3 (2019). [PubMed: 30980069]
6. Cameron DR, Shan Y, Zalis EA, Isabella V & Lewis K A Genetic Determinant of Persister Cell Formation in Bacterial Pathogens. J Bacteriol 200, doi:10.1128/JB.00303-18 (2018).
7. Scherr TD et al. Staphylococcus aureus Biofilms Induce Macrophage Dysfunction Through Leukocidin AB and Alpha-Toxin. MBio 6, doi:10.1128/mBio.01021-15 (2015).
8. Koziel J et al. The Janus face of alpha-toxin: a potent mediator of cytoprotection in staphylococci-infected macrophages. J Innate Immun 7, 187–198, doi:10.1159/000368048 (2015). [PubMed: 25358860]
9. Schommer NN et al. Staphylococcus epidermidis uses distinct mechanisms of biofilm formation to interfere with phagocytosis and activation of mouse macrophage-like cells 774A.1. Infect Immun 79, 2267–2276, doi:10.1128/IAI.01142-10 (2011). [PubMed: 21402760]
10. Thurlow LR et al. Staphylococcus aureus biofilms prevent macrophage phagocytosis and attenuate inflammation in vivo. J Immunol 186, 6585–6596, doi:10.4049/jimmunol.1002794 (2011). [PubMed: 21525381]
11. Ricciardi BF et al. Staphylococcus aureus Evasion of Host Immunity in the Setting of Prosthetic Joint Infection: Biofilm and Beyond. Curr Rev Musculoskelet Med 11, 389–400, doi:10.1007/s12178-018-9501-4 (2018). [PubMed: 29987645]
12. Le KY, Park MD & Otto M Immune Evasion Mechanisms of Staphylococcus epidermidis Biofilm Infection. Front Microbiol 9, 359, doi:10.3389/fmicb.2018.00359 (2018). [PubMed: 29541068]
13. He L et al. Resistance to leukocytes ties benefits of quorum sensing dysfunctionality to biofilm infection. Nature microbiology 4, 1114–1119, doi:10.1038/s41564-019-0413-x (2019).
14. Heim CE et al. Myeloid-derived suppressor cells contribute to Staphylococcus aureus orthopedic biofilm infection. J Immunol 192, 3778–3792, doi:10.4049/jimmunol.1303408 (2014). [PubMed: 24646737]
15. Heim CE et al. IL-12 promotes myeloid-derived suppressor cell recruitment and bacterial persistence during Staphylococcus aureus orthopedic implant infection. J Immunol 194, 3861–3872, doi:10.4049/jimmunol.1402689 (2015). [PubMed: 25762781]
16. Heim CE, Vidlak D & Kielian T Interleukin-10 production by myeloid-derived suppressor cells contributes to bacterial persistence during Staphylococcus aureus orthopedic biofilm infection. J Leukoc Biol 98, 1003–1013, doi:10.1189/jlb.4VMA0315-125RR (2015). [PubMed: 26232453]
17. Tebartz C et al. A major role for myeloid-derived suppressor cells and a minor role for regulatory T cells in immunosuppression during Staphylococcus aureus infection. J Immunol 194, 1100–1111, doi:10.4049/jimmunol.1400196 (2015). [PubMed: 25548227]
18. Bernthal NM et al. Protective role of IL-1beta against post-arthroplasty Staphylococcus aureus infection. J Orthop Res 29, 1621–1626, doi:10.1002/jor.21414 (2011). [PubMed: 21445990]
19. Ouyang W & O'Garra A IL-10 Family Cytokines IL-10 and IL-22: from Basic Science to Clinical Translation. Immunity 50, 871–891, doi:10.1016/j.immuni.2019.03.020 (2019). [PubMed: 30995504]

20. Kessler B et al. Interleukin 10 inhibits pro-inflammatory cytokine responses and killing of Burkholderia pseudomallei. Sci Rep 7, 42791, doi:10.1038/srep42791 (2017). [PubMed: 28216665]
21. Leech JM, Lacey KA, Mulcahy ME, Medina E & McLoughlin RM IL-10 Plays Opposing Roles during Staphylococcus aureus Systemic and Localized Infections. J Immunol 198, 2352–2365, doi:10.4049/jimmunol.1601018 (2017). [PubMed: 28167629]
22. Alter G et al. IL-10 induces aberrant deletion of dendritic cells by natural killer cells in the context of HIV infection. J Clin Invest 120, 1905–1913, doi:10.1172/JCI40913 (2010). [PubMed: 20440075]
23. Smith LK et al. Interleukin-10 Directly Inhibits CD8(+) T Cell Function by Enhancing N-Glycan Branching to Decrease Antigen Sensitivity. Immunity 48, 299–312 e295, doi:10.1016/j.immuni.2018.01.006 (2018). [PubMed: 29396160]
24. Akdis CA, Joss A, Akdis M, Faith A & Blaser K A molecular basis for T cell suppression by IL-10: CD28-associated IL-10 receptor inhibits CD28 tyrosine phosphorylation and phosphatidylinositol 3-kinase binding. FASEB J 14, 1666–1668, doi:10.1096/fj.99-0874fje (2000). [PubMed: 10973911]
25. Liu B, Tonkonogy SL & Sartor RB Antigen-presenting cell production of IL-10 inhibits T-helper 1 and 17 cell responses and suppresses colitis in mice. Gastroenterology 141, 653–662, 662 e651–654, doi:10.1053/j.gastro.2011.04.053 (2011). [PubMed: 21679711]
26. Sinha P, Clements VK, Bunt SK, Albelda SM & Ostrand-Rosenberg S Cross-talk between myeloid-derived suppressor cells and macrophages subverts tumor immunity toward a type 2 response. J Immunol 179, 977–983, doi:10.4049/jimmunol.179.2.977 (2007). [PubMed: 17617589]
27. Beury DW et al. Cross-talk among myeloid-derived suppressor cells, macrophages, and tumor cells impacts the inflammatory milieu of solid tumors. J Leukoc Biol 96, 1109–1118, doi:10.1189/jlb.3A0414-210R (2014). [PubMed: 25170116]
28. Fey PD et al. A genetic resource for rapid and comprehensive phenotype screening of nonessential Staphylococcus aureus genes. MBio 4, e00537–00512, doi:10.1128/mBio.00537-12 (2013). [PubMed: 23404398]
29. Fuller JR et al. Identification of a lactate-quinone oxidoreductase in Staphylococcus aureus that is essential for virulence. Front Cell Infect Microbiol 1, 19, doi:10.3389/fcimb.2011.00019 (2011). [PubMed: 22919585]
30. Stockland AE & San Clemente CL Multiple forms of lactate dehydrogenase in Staphylococcus aureus. J Bacteriol 100, 347–353 (1969). [PubMed: 4310081]
31. Kondoh Y, Kawase M, Kawakami Y & Ohmori S Concentrations of D-lactate and its related metabolic intermediates in liver, blood, and muscle of diabetic and starved rats. Res Exp Med (Berl) 192, 407–414 (1992). [PubMed: 1480818]
32. Puig-Kroger A et al. Peritoneal dialysis solutions inhibit the differentiation and maturation of human monocyte-derived dendritic cells: effect of lactate and glucose-degradation products. J Leukoc Biol 73, 482–492, doi:10.1189/jlb.0902451 (2003). [PubMed: 12660223]
33. Husain Z, Huang Y, Seth P & Sukhatme VP Tumor-derived lactate modifies antitumor immune response: effect on myeloid-derived suppressor cells and NK cells. J Immunol 191, 1486–1495, doi:10.4049/jimmunol.1202702 (2013). [PubMed: 23817426]
34. Zhang D et al. Metabolic regulation of gene expression by histone lactylation. Nature 574, 575–580, doi:10.1038/s41586-019-1678-1 (2019). [PubMed: 31645732]
35. Ratter JM et al. In vitro and in vivo Effects of Lactate on Metabolism and Cytokine Production of Human Primary PBMCs and Monocytes. Front Immunol 9, 2564, doi:10.3389/fimmu.2018.02564 (2018). [PubMed: 30483253]
36. Latham T et al. Lactate, a product of glycolytic metabolism, inhibits histone deacetylase activity and promotes changes in gene expression. Nucleic Acids Res 40, 4794–4803, doi:10.1093/nar/gks066 (2012). [PubMed: 22323521]
37. Wagner W, Ciszewski WM & Kania KD L- and D-lactate enhance DNA repair and modulate the resistance of cervical carcinoma cells to anticancer drugs via histone deacetylase inhibition and

hydroxycarboxylic acid receptor 1 activation. Cell Commun Signal 13, 36, doi:10.1186/s12964-015-0114-x (2015). [PubMed: 26208712]

38. Strahl BD & Allis CD The language of covalent histone modifications. Nature 403, 41–45, doi:10.1038/47412 (2000). [PubMed: 10638745]
39. Shakespear MR, Halili MA, Irvine KM, Fairlie DP & Sweet MJ Histone deacetylases as regulators of inflammation and immunity. Trends Immunol 32, 335–343, doi:10.1016/j.it.2011.04.001 (2011). [PubMed: 21570914]
40. Cheng F et al. Divergent roles of histone deacetylase 6 (HDAC6) and histone deacetylase 11 (HDAC11) on the transcriptional regulation of IL10 in antigen presenting cells. Mol Immunol 60, 44–53, doi:10.1016/j.molimm.2014.02.019 (2014). [PubMed: 24747960]
41. Villagra A et al. The histone deacetylase HDAC11 regulates the expression of interleukin 10 and immune tolerance. Nat Immunol 10, 92–100, doi:10.1038/ni.1673 (2009). [PubMed: 19011628]
42. Garvie EI Bacterial lactate dehydrogenases. Microbiol Rev 44, 106–139 (1980). [PubMed: 6997721]
43. Gaspar P, Al-Bayati FA, Andrew PW, Neves AR & Yesilkaya H Lactate dehydrogenase is the key enzyme for pneumococcal pyruvate metabolism and pneumococcal survival in blood. Infect Immun 82, 5099–5109, doi:10.1128/IAI.02005-14 (2014). [PubMed: 25245810]
44. Bunch PK, Mat-Jan F, Lee N & Clark DP The ldhA gene encoding the fermentative lactate dehydrogenase of Escherichia coli. Microbiology 143 (Pt 1), 187–195, doi:10.1099/00221287-143-1-187 (1997). [PubMed: 9025293]
45. Feldman-Salit A et al. Regulation of the activity of lactate dehydrogenases from four lactic acid bacteria. J Biol Chem 288, 21295–21306, doi:10.1074/jbc.M113.458265 (2013). [PubMed: 23720742]
46. Spahich NA, Vitko NP, Thurlow LR, Temple B & Richardson AR Staphylococcus aureus lactate- and malate-quinone oxidoreductases contribute to nitric oxide resistance and virulence. Mol Microbiol 100, 759–773, doi:10.1111/mmi.13347 (2016). [PubMed: 26851155]
47. Bola BM et al. Inhibition of monocarboxylate transporter-1 (MCT1) by AZD3965 enhances radiosensitivity by reducing lactate transport. Mol Cancer Ther 13, 2805–2816, doi:10.1158/1535-7163.MCT-13-1091 (2014). [PubMed: 25281618]
48. Wang Q et al. Characterization of monocarboxylate transport in human kidney HK-2 cells. Mol Pharm 3, 675–685, doi:10.1021/mp060037b (2006). [PubMed: 17140255]
49. Polanski R et al. Activity of the monocarboxylate transporter 1 inhibitor AZD3965 in small cell lung cancer. Clin Cancer Res 20, 926–937, doi:10.1158/1078-0432.CCR-13-2270 (2014). [PubMed: 24277449]
50. Corbet C et al. Interruption of lactate uptake by inhibiting mitochondrial pyruvate transport unravels direct antitumor and radiosensitizing effects. Nat Commun 9, 1208, doi:10.1038/s41467-018-03525-0 (2018). [PubMed: 29572438]
51. Garcia-Castillo V et al. Targeting Metabolic Remodeling in Triple Negative Breast Cancer in a Murine Model. J Cancer 8, 178–189, doi:10.7150/jca.16387 (2017). [PubMed: 28243322]
52. Zhao Z, Han F, Yang S, Wu J & Zhan W Oxamate-mediated inhibition of lactate dehydrogenase induces protective autophagy in gastric cancer cells: involvement of the Akt-mTOR signaling pathway. Cancer Lett 358, 17–26, doi:10.1016/j.canlet.2014.11.046 (2015). [PubMed: 25524555]
53. Zhai X, Yang Y, Wan J, Zhu R & Wu Y Inhibition of LDH-A by oxamate induces G2/M arrest, apoptosis and increases radiosensitivity in nasopharyngeal carcinoma cells. Oncol Rep 30, 2983–2991, doi:10.3892/or.2013.2735 (2013). [PubMed: 24064966]
54. Askarian F, Wagner T, Johannessen M & Nizet V Staphylococcus aureus modulation of innate immune responses through Toll-like (TLR), (NOD)-like (NLR) and C-type lectin (CLR) receptors. FEMS Microbiol Rev 42, 656–671, doi:10.1093/femsre/fuy025 (2018). [PubMed: 29893825]
55. Hanzelmann D et al. Toll-like receptor 2 activation depends on lipopeptide shedding by bacterial surfactants. Nat Commun 7, 12304, doi:10.1038/ncomms12304 (2016). [PubMed: 27470911]
56. Kawasaki T & Kawai T Toll-like receptor signaling pathways. Front Immunol 5, 461, doi:10.3389/fimmu.2014.00461 (2014). [PubMed: 25309543]

57. Larsson L, Thorbert-Mros S, Rymo L & Berglundh T Influence of epigenetic modifications of the interleukin-10 promoter on IL10 gene expression. Eur J Oral Sci 120, 14–20, doi:10.1111/j.1600-0722.2011.00917.x (2012). [PubMed: 22288916]
58. Yuan ZL, Guan YJ, Chatterjee D & Chin YE Stat3 dimerization regulated by reversible acetylation of a single lysine residue. Science 307, 269–273, doi:10.1126/science.1105166 (2005). [PubMed: 15653507]
59. Qin G et al. Metformin blocks myeloid-derived suppressor cell accumulation through AMPK-DACH1-CXCL1 axis. Oncoimmunology 7, e1442167, doi:10.1080/2162402X.2018.1442167 (2018). [PubMed: 29900050]
60. Ouzounova M et al. Monocytic and granulocytic myeloid derived suppressor cells differentially regulate spatiotemporal tumour plasticity during metastatic cascade. Nat Commun 8, 14979, doi:10.1038/ncomms14979 (2017). [PubMed: 28382931]
61. Zhang CX et al. STING signaling remodels the tumor microenvironment by antagonizing myeloid-derived suppressor cell expansion. Cell Death Differ, doi:10.1038/s41418-019-0302-0 (2019).
62. Sundaram K et al. IkappaBzeta Regulates Human Monocyte Pro-Inflammatory Responses Induced by Streptococcus pneumoniae. PLoS One 11, e0161931, doi:10.1371/journal.pone.0161931 (2016). [PubMed: 27597997]
63. Katoh H et al. CXCR2-expressing myeloid-derived suppressor cells are essential to promote colitis-associated tumorigenesis. Cancer Cell 24, 631–644, doi:10.1016/j.ccr.2013.10.009 (2013). [PubMed: 24229710]
64. Li W, Mao Z, Fan X, Cui L & Wang X Cyclooxygenase 2 promoted the tumorigenecity of pancreatic cancer cells. Tumour Biol 35, 2271–2278, doi:10.1007/s13277-013-1301-2 (2014). [PubMed: 24146280]
65. Lucas M, Zhang X, Prasanna V & Mosser DM ERK activation following macrophage FcgammaR ligation leads to chromatin modifications at the IL-10 locus. J Immunol 175, 469–477, doi:10.4049/jimmunol.175.1.469 (2005). [PubMed: 15972681]
66. Turner BM Cellular memory and the histone code. Cell 111, 285–291, doi:10.1016/s0092-8674(02)01080-2 (2002). [PubMed: 12419240]
67. Youn JI et al. Epigenetic silencing of retinoblastoma gene regulates pathologic differentiation of myeloid cells in cancer. Nat Immunol 14, 211–220, doi:10.1038/ni.2526 (2013). [PubMed: 23354483]
68. Rosborough BR, Castellaneta A, Natarajan S, Thomson AW & Turnquist HR Histone deacetylase inhibition facilitates GM-CSF-mediated expansion of myeloid-derived suppressor cells in vitro and in vivo. J Leukoc Biol 91, 701–709, doi:10.1189/jlb.0311119 (2012). [PubMed: 22028329]
69. Sahakian E et al. Histone deacetylase 11: A novel epigenetic regulator of myeloid derived suppressor cell expansion and function. Mol Immunol 63, 579–585, doi:10.1016/j.molimm.2014.08.002 (2015). [PubMed: 25155994]
70. Eskandarian HA et al. A role for SIRT2-dependent histone H3K18 deacetylation in bacterial infection. Science 341, 1238858, doi:10.1126/science.1238858 (2013). [PubMed: 23908241]
71. Kincaid EZ & Ernst JD Mycobacterium tuberculosis exerts gene-selective inhibition of transcriptional responses to IFN-gamma without inhibiting STAT1 function. J Immunol 171, 2042–2049, doi:10.4049/jimmunol.171.4.2042 (2003). [PubMed: 12902509]
72. Wang Y, Curry HM, Zwilling BS & Lafuse WP Mycobacteria inhibition of IFN-gamma induced HLA-DR gene expression by up-regulating histone deacetylation at the promoter region in human THP-1 monocytic cells. J Immunol 174, 5687–5694, doi:10.4049/jimmunol.174.9.5687 (2005). [PubMed: 15843570]
73. Pathak SK et al. TLR4-dependent NF-kappaB activation and mitogen- and stress-activated protein kinase 1-triggered phosphorylation events are central to Helicobacter pylori peptidyl prolyl cis-, trans-isomerase (HP0175)-mediated induction of IL-6 release from macrophages. J Immunol 177, 7950–7958, doi:10.4049/jimmunol.177.11.7950 (2006). [PubMed: 17114467]
74. Cao J et al. HDAC11 regulates type I interferon signaling through defatty-acylation of SHMT2. Proc Natl Acad Sci U S A 116, 5487–5492, doi:10.1073/pnas.1815365116 (2019). [PubMed: 30819897]

75. Moreno-Yruela C, Galleano I, Madsen AS & Olsen CA Histone Deacetylase 11 Is an epsilon-N-Myristoyllysine Hydrolase. Cell Chem Biol 25, 849–856 e848, doi:10.1016/j.chembiol.2018.04.007 (2018). [PubMed: 29731425]
76. Kutil Z et al. Histone Deacetylase 11 Is a Fatty-Acid Deacylase. ACS Chem Biol 13, 685–693, doi:10.1021/acschembio.7b00942 (2018). [PubMed: 29336543]
77. Korkmaz B, Horwitz MS, Jenne DE & Gauthier F Neutrophil elastase, proteinase 3, and cathepsin G as therapeutic targets in human diseases. Pharmacol Rev 62, 726–759, doi:10.1124/pr.110.002733 (2010). [PubMed: 21079042]
78. Lau D et al. Myeloperoxidase mediates neutrophil activation by association with CD11b/CD18 integrins. Proc Natl Acad Sci U S A 102, 431–436, doi:10.1073/pnas.0405193102 (2005). [PubMed: 15625114]
79. Kumar V, Patel S, Tcyganov E & Gabrilovich DI The Nature of Myeloid-Derived Suppressor Cells in the Tumor Microenvironment. Trends Immunol 37, 208–220, doi:10.1016/j.it.2016.01.004 (2016). [PubMed: 26858199]
80. Obermajer N & Kalinski P Key role of the positive feedback between PGE(2) and COX2 in the biology of myeloid-derived suppressor cells. Oncoimmunology 1, 762–764, doi:10.4161/onci.19681 (2012). [PubMed: 22934275]
81. Dufait I et al. Perforin and Granzyme B Expressed by Murine Myeloid-Derived Suppressor Cells: A Study on Their Role in Outgrowth of Cancer Cells. Cancers 11, doi:10.3390/cancers11060808 (2019).
82. Sawant A et al. Myeloid-derived suppressor cells function as novel osteoclast progenitors enhancing bone loss in breast cancer. Cancer Res 73, 672–682, doi:10.1158/0008-5472.CAN-12-2202 (2013). [PubMed: 23243021]
83. Heim CE et al. Human prosthetic joint infections are associated with myeloid-derived suppressor cells (MDSCs): Implications for infection persistence. J Orthop Res 36, 1605–1613, doi:10.1002/jor.23806 (2018). [PubMed: 29139571]
84. Manning Fox JE, Meredith D & Halestrap AP Characterisation of human monocarboxylate transporter 4 substantiates its role in lactic acid efflux from skeletal muscle. J Physiol 529 Pt 2, 285–293, doi:10.1111/j.1469-7793.2000.00285.x (2000). [PubMed: 11101640]
85. Vitko NP, Grosser MR, Khatri D, Lance TR & Richardson AR Expanded Glucose Import Capability Affords Staphylococcus aureus Optimized Glycolytic Flux during Infection. MBio 7, doi:10.1128/mBio.00296-16 (2016).
86. Vitko NP, Spahich NA & Richardson AR Glycolytic dependency of high-level nitric oxide resistance and virulence in Staphylococcus aureus. MBio 6, doi:10.1128/mBio.00045-15 (2015).
87. Yermak K, Karbysheva S, Perka C, Trampuz A & Renz N Performance of synovial fluid D-lactate for the diagnosis of periprosthetic joint infection: A prospective observational study. J Infect, doi:10.1016/j.jinf.2019.05.015 (2019).
88. Zhang Q & Cao X Epigenetic regulation of the innate immune response to infection. Nat Rev Immunol 19, 417–432, doi:10.1038/s41577-019-0151-6 (2019). [PubMed: 30918351]
89. Turner NA et al. Methicillin-resistant Staphylococcus aureus: an overview of basic and clinical research. Nat Rev Microbiol 17, 203–218, doi:10.1038/s41579-018-0147-4 (2019). [PubMed: 30737488]
90. Sun L et al. Loss of HDAC11 ameliorates clinical symptoms in a multiple sclerosis mouse model. Life Sci Alliance 1, e201800039, doi:10.26508/lsa.201800039 (2018). [PubMed: 30456376]
91. Mootz JM, Malone CL, Shaw LN & Horswill AR Staphopains modulate Staphylococcus aureus biofilm integrity. Infect Immun 81, 3227–3238, doi:10.1128/IAI.00377-13 (2013). [PubMed: 23798534]
92. Gries CM et al. Cyclic di-AMP Released from Staphylococcus aureus Biofilm Induces a Macrophage Type I Interferon Response. Infect Immun 84, 3564–3574, doi:10.1128/IAI.00447-16 (2016). [PubMed: 27736778]
93. Yamada KJ et al. Arginase-1 Expression in Myeloid Cells Regulates Staphylococcus aureus Planktonic but Not Biofilm Infection. Infect Immun 86, doi:10.1128/IAI.00206-18 (2018).

94. Heim CE, West SC, Ali H & Kielian T Heterogeneity of Ly6G(+) Ly6C(+) Myeloid-Derived Suppressor Cell Infiltrates during Staphylococcus aureus Biofilm Infection. Infect Immun 86, doi:10.1128/IAI.00684-18 (2018).

95. Niska JA et al. Vancomycin-rifampin combination therapy has enhanced efficacy against an experimental Staphylococcus aureus prosthetic joint infection. Antimicrob Agents Chemother 57, 5080–5086, doi:10.1128/AAC.00702-13 (2013). [PubMed: 23917317]

96. Pribaz JR et al. Mouse model of chronic post-arthroplasty infection: noninvasive in vivo bioluminescence imaging to monitor bacterial burden for long-term study. J Orthop Res 30, 335–340, doi:10.1002/jor.21519 (2012). [PubMed: 21837686]

97. Niska JA et al. Monitoring bacterial burden, inflammation and bone damage longitudinally using optical and muCT imaging in an orthopaedic implant infection in mice. PLoS One 7, e47397, doi:10.1371/journal.pone.0047397 (2012). [PubMed: 23082163]

98. Yamada KJ et al. Monocyte metabolic reprogramming promotes pro-inflammatory activity and Staphylococcus aureus biofilm clearance. PLoS Pathog 16, e1008354, doi:10.1371/journal.ppat.1008354 (2020). [PubMed: 32142554]

99. Langmead B & Salzberg SL Fast gapped-read alignment with Bowtie 2. Nat Methods 9, 357–359, doi:10.1038/nmeth.1923 (2012). [PubMed: 22388286]

100. Allhoff M, Sere K, J FP, Zenke M & I GC Differential peak calling of ChIP-seq signals with replicates with THOR. Nucleic Acids Res 44, e153, doi:10.1093/nar/gkw680 (2016). [PubMed: 27484474]

101. Allhoff M et al. Detecting differential peaks in ChIP-seq signals with ODIN. Bioinformatics 30, 3467–3475, doi:10.1093/bioinformatics/btu722 (2014). [PubMed: 25371479]

102. Lin X, Tirichine L & Bowler C Protocol: Chromatin immunoprecipitation (ChIP) methodology to investigate histone modifications in two model diatom species. Plant Methods 8, 48, doi:10.1186/1746-4811-8-48 (2012). [PubMed: 23217141]

103. Pfaffl MW A new mathematical model for relative quantification in real-time RT-PCR. Nucleic Acids Res 29, e45, doi:10.1093/nar/29.9.e45 (2001). [PubMed: 11328886]

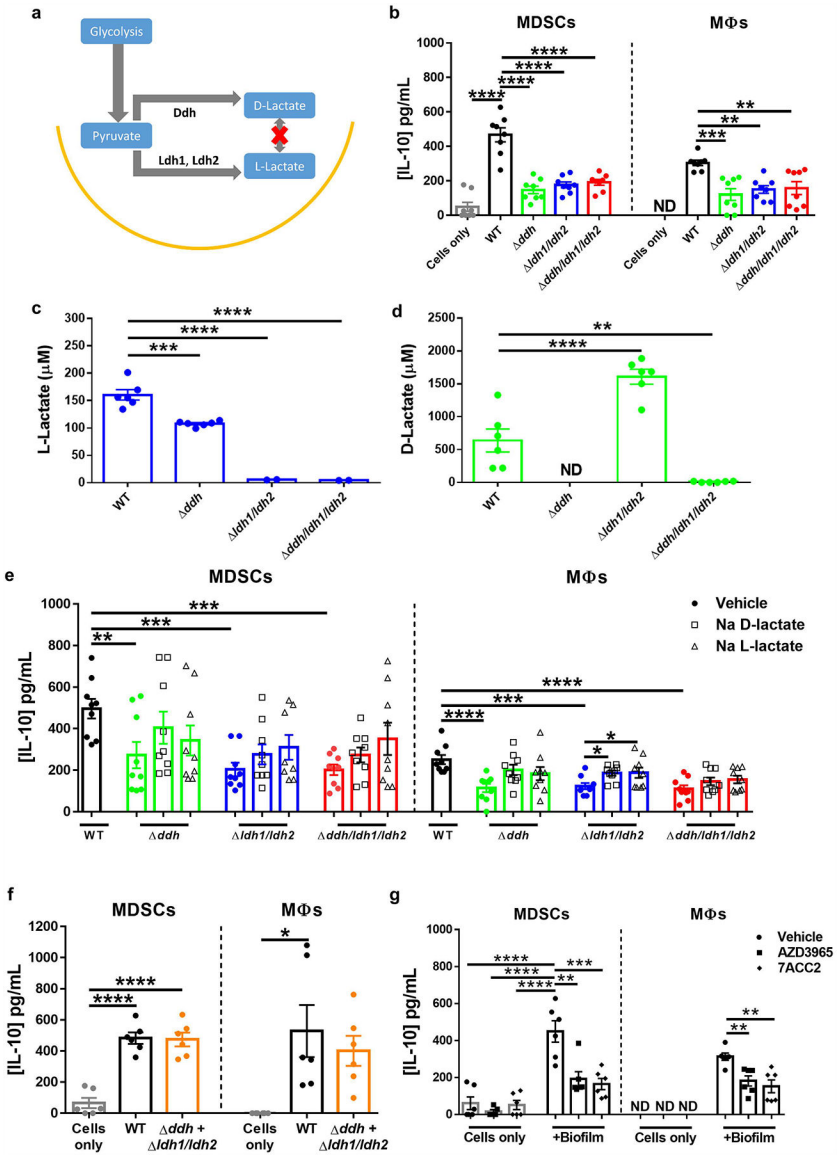

Figure 1. Lactate biosynthesis pathways induce MDSC and macrophage IL-10 production.

(**a**) Enzymes responsible for D- and L-lactate production in *S. aureus*. (**b**) MDSC and macrophage IL-10 release elicited from WT and lactate mutant biofilm. (**c**) L- and (**d**) D-lactate production by *S. aureus* WT and lactate mutant biofilm. (**e**) Sodium D- or L-lactate (2.5 μM) was added to lactate mutant biofilms during a 2 h co-culture with MDSCs or macrophages. (**f**) A Δ*ddh* and Δ*ldh1/ldh2* mixed biofilm reveals the requirement for both D- and L-lactate for maximal IL-10 production. (**g**) MCT-1 inhibitors (AZD3965 and 7ACC2, both at 10 nM) were added during a 2 h co-culture with WT biofilm. IL-10 levels were measured for all experiments by ELISA. Results are reported as (**b**) the mean ± SEM from two independent experiments each with four biological replicates; (**c** and **d**) two independent experiments, each with three biological replicates; and (**e**) two (macrophages) and three (MDSCs) independent experiments, each with three biological replicates; and two (**f, g**)

independent experiments, each with three biological replicates. ND, not detected. *, $p < 0.05$; **, $p < 0.01$; ***, $p < 0.001$; ****, $p < 0.0001$; One-way ANOVA.

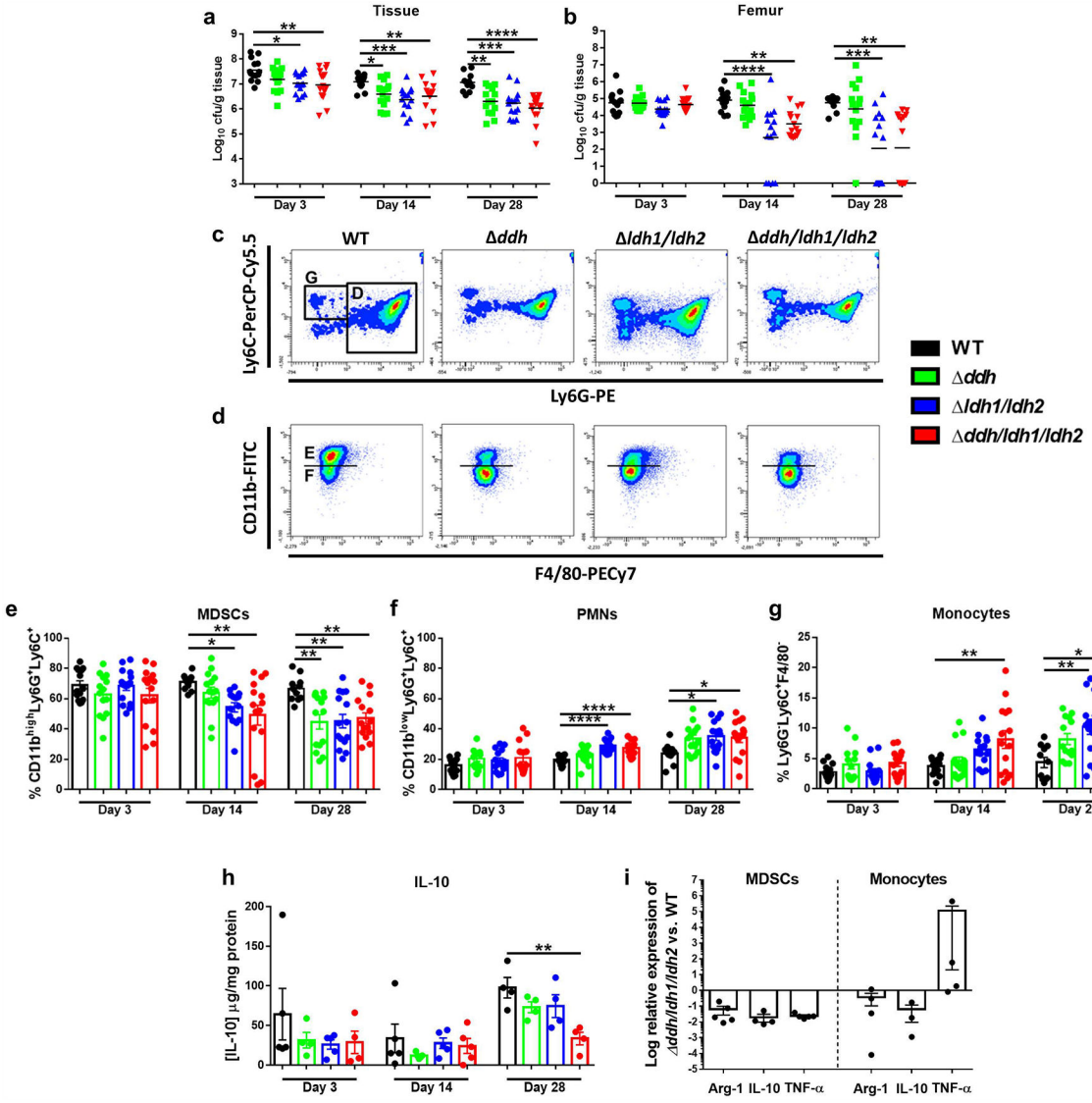

Figure 2. Role for Ddh, Ldh1, and Ldh2 during *S. aureus* orthopaedic implant infection.

Implant-associated tissues were collected at days 3, 14, and 28 post-infection, whereupon bacterial burden was quantified in (**a**) implant-associated soft tissue and (**b**) femur of mice infected with WT, Δ*ddh*, Δ*ldh1/ldh2*, and Δ*ddh/ldh1/ldh2*. (**c**) Representative contour plots of Ly6G and Ly6C staining demonstrate the abundance of $Ly6G^{+}Ly6C^{+}$ (inset D) and $Ly6G^{-}Ly6C^{+}$ cells (inset G) in WT or lactate mutant tissues at day 28 post-infection. (**d**) CD11b expression of $Ly6G^{+}Ly6C^{+}$ cells depicted in inset D, where the horizontal line demarcates $CD11b^{high}$ MDSCs from $CD11b^{low}$ PMNs. Quantification of (**e**) $CD11b^{high}Ly6G^{+}Ly6C^{+}$ MDSCs (**f**) $CD11b^{low}Ly6G^{+}Ly6C^{+}$ PMNs, and (**g**) $Ly6G^{-}Ly6C^{+}F4/80^{-}$ monocytes in infected tissue. (**h**) IL-10 levels in implant-associated tissue were measured by ELISA. (**i**) Gene expression in $CD11b^{high}Ly6G^{+}Ly6C^{+}$ MDSCs or $Ly6G^{-}Ly6C^{+}F4/80^{-}$ monocytes purified from implant-associated tissue of WT and Δ*ddh/ldh1/ldh2*-infected mice at day 3 by FACS, with results presented as the fold-change in Δ*ddh/ldh1/ldh2* MDSCs or monocytes relative to leukocytes from WT-infected animals. Results represent (**a-b and e-g**) the mean ±

SEM of three independent experiments (Day 3, n=14 for WT and Δ*ddh* and 15 for Δ*ldh1/ldh2* and Δ*ddh/ldh1/ldh2*; Day 14, n=15/strain; Day 28, n=11 for WT, 14 for Δ*ddh*, and 15 for Δ*ldh1/ldh2* and Δ*ddh/ldh1/ldh2*), (**c and d**) representative plots from three independent experiments, (**h**) mean ± SD of one representative experiment (Day 3, n=5 for WT and Δ*ldh1/ldh2* and 4 for Δ*ddh* and Δ*ddh/ldh1/ldh2*; Day 14, n=5/strain; Day 28, n=4/strain) performed three times, or (**i**) the mean ± SEM of two independent experiments for MDSCs [n=4 (IL-10) and 5 (Arg-1 and TNF-α) biological replicates] and macrophages [n=3 (IL-10) and 4 (Arg-1 and TNF-α) biological replicates]. *, $p < 0.05$; **, $p < 0.01$; ***, $p < 0.001$; ****, $p < 0.0001$; One-way ANOVA.

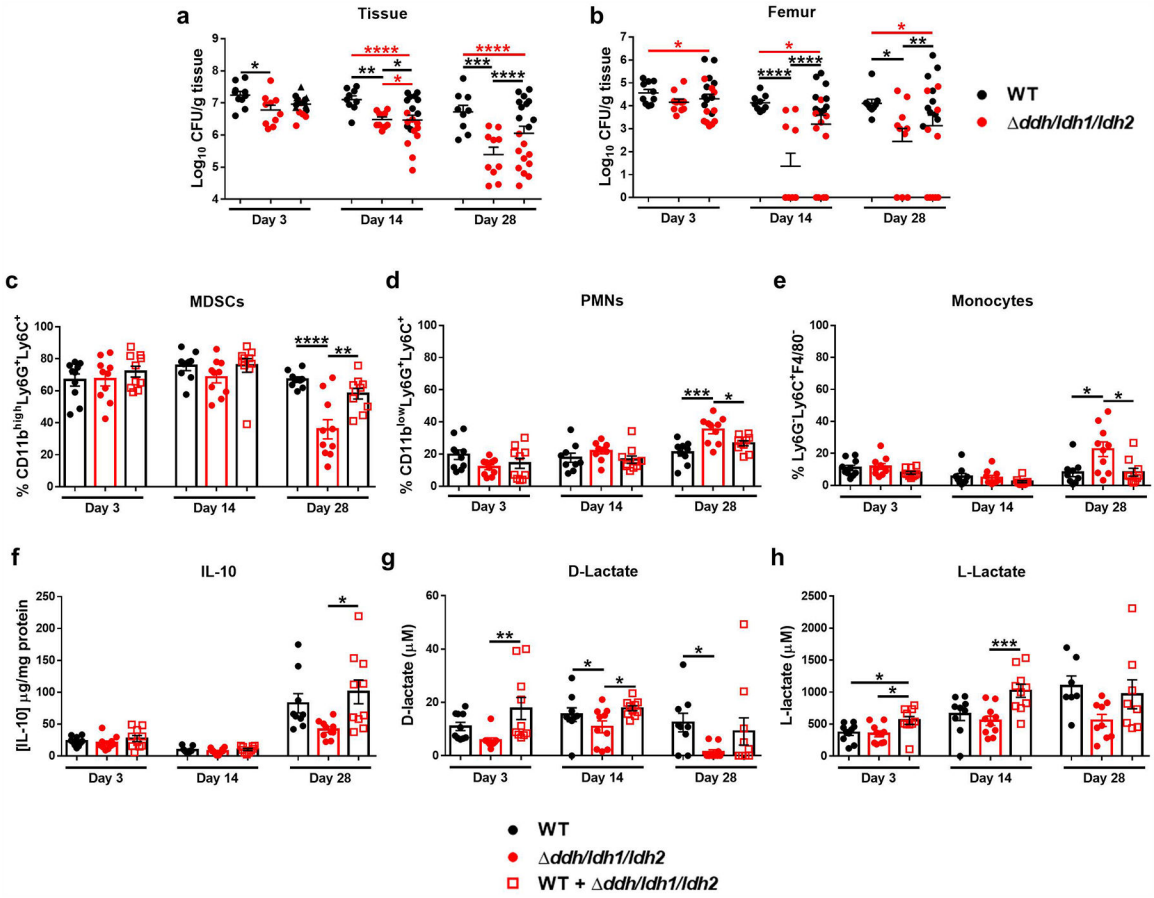

Figure 3. *S. aureus* lactate promotes IL-10 production and regulates leukocyte infiltrates during PJI.

Mice were infected with WT, Δ*ddh/ldh1/ldh2*, or a 1:1 ratio of WT and Δ*ddh/ldh1/ldh2*, whereupon tissues were collected at days 3, 14, and 28 post-infection to quantify bacterial burden in the (**a**) implant-associated soft tissue and (**b**) femur. Quantification of (**c**) $CD11b^{high}Ly6G^{+}Ly6C^{+}$ MDSCs (**d**) $CD11b^{low}Ly6G^{+}Ly6C^{+}$ PMNs, (**e**) $Ly6G^{-}Ly6C^{+}F4/80^{-}$ monocytes, (**f**) IL-10, (**g**) D-lactate, and (**h**) L-lactate in implant-associated tissue. Results are combined from two independent experiments (Day 3, n=10/group; Day 14, n=9 for WT and 10 for Δ*ddh/ldh1/ldh2* and WT+Δ*ddh/ldh1/ldh2*; Day 28, n=9 for WT and 10 for Δ*ddh/ldh1/ldh2* and WT+Δ*ddh/ldh1/ldh2*). *, $p < 0.05$; **, $p < 0.01$; ***, $p < 0.001$; ****, $p < 0.0001$; One-way ANOVA. In (**a**) and (**b**), black asterisks indicate significant differences between WT bacteria across all groups and red asterisks reflect significant differences between Δ*ddh/ldh1/ldh2* across all groups.

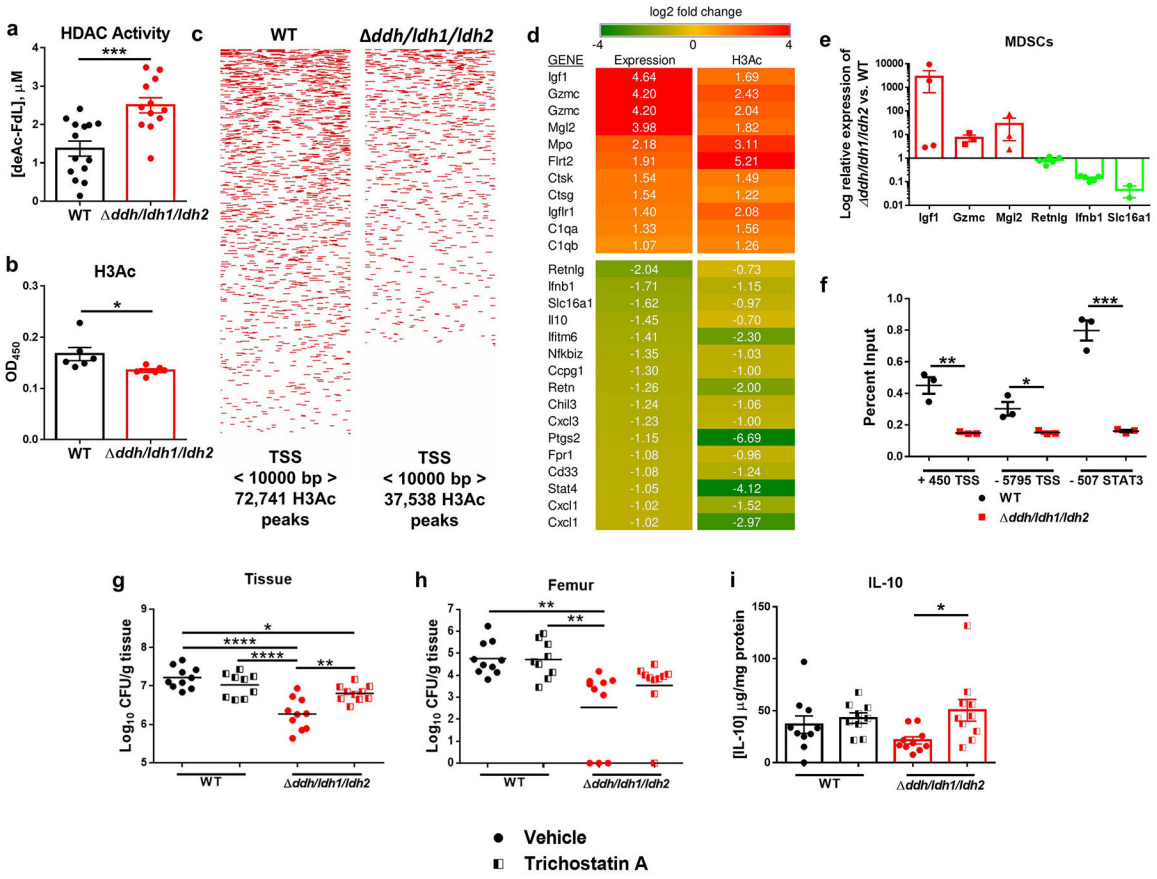

Figure 4. *S. aureus*-derived lactate inhibits HDAC activity to regulate Histone 3 (H3) acetylation and gene expression.

Total leukocytes were recovered from WT (n=14 biological replicates) and Δ*ddh/ldh1/ldh2*-infected mice (n=12 biological replicates) at day 14 and assessed for (**a**) HDAC activity using a fluorescent HDAC substrate (deAc-FdL; two independent experiments; ***, p = 0.0005) and (**b**) relative abundance of acetylated Histone 3 (H3Ac) by ELISA (mean ± SD from six biological replicates; *, p = 0.0365). (**c**) Significant changes in H3Ac peaks ± 10,000 bp of the transcriptional start site (TSS) as identified by ChIP-seq in purified MDSCs collected at day 14 post-infection (two independent experiments with cells pooled from 15 mice per experiment). (**d**) Genes identified by single cell RNA-seq (total $CD45^+$ leukocytes collected from 3 mice) with concordant changes in H3Ac status as determined in (**c**) with results expressed as the fold-change in leukocytes recovered from Δ*ddh/ldh1/ldh2* vs. WT infected mice. Genes that appear more than once reflect those with multiple altered H3Ac ChIP peaks. (**e**) RT-qPCR validation of the top 3 upregulated and downregulated genes identified in (**d**) in purified MDSCs collected at day 14 post-infection (two independent experiments; n= 5 but some genes did not amplify in all samples). (**f**) ChIP-qPCR for H3Ac within three regions associated with the IL-10 promoter in purified MDSCs at day 14 after infection (n= 3 technical replicates from MDSCs that were pooled from 25 mice/group over 3 independent experiments due to limiting input ChIP DNA from low cell yields). **, p = 0.0046;*, p = 0.0261; and ***, p = 0.0006, respectively). (**g-i**) WT or Δ*ddh/ldh1/ldh2*-infected mice were treated with vehicle (n=10/group) or 0.5 mg/kg of the pan-HDACi

trichostatin A (n=9 or 10 for WT and Δ*ddh/ldh1/ldh2*, respectively) once daily, and sacrificed at day 14 post-infection for quantification of bacterial burden in (**g**) implant-associated tissue and (**h**) femur, and (**i**) IL-10 in infected tissue. Results are representative of two independent experiments. Results in panels **a**, **b**, and **f** were analyzed using an unpaired two-tailed Student's *t*-test and panels **g-i** by One-way ANOVA (*, $p < 0.05$; **, $p < 0.01$; ****, $p < 0.0001$). The results in **c** reflect a *p*-value < 0.05 as determined using a statistical test for each ChIP-enriched region as described in[100] and corrected using the Benjamini and Hochberg method to control for False Discovery Rate.

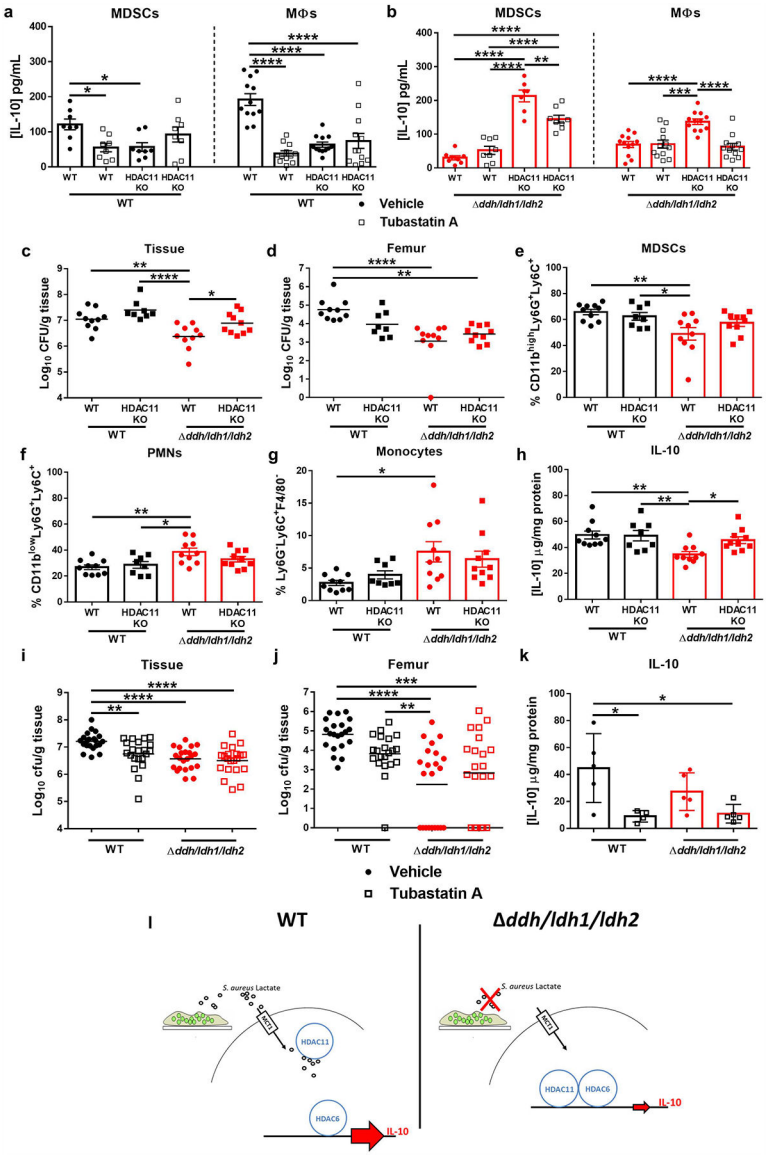

Figure 5. *S. aureus*-derived lactate inhibits the negative regulator HDAC11 to augment leukocyte IL-10 production in a HDAC6-dependent manner.

(**a and b**) MDSCs and macrophages from WT or HDAC11 KO mice were co-cultured with WT or Δ*ddh/ldh1/ldh2* biofilm for 2 h in the presence or absence of the HDAC6i tubastatin A (15 nM), whereupon IL-10 production was measured by cytometric bead array. Results represent the mean ± SEM combined from two independent experiments (n=8 and 12 biological replicates for MDSCs and macrophages, respectively, except for WT MDSCs + tubastatin A in **b** where n=7). (**c-h**) WT and HDAC11 KO mice were infected with *S. aureus* WT (n=10 and 8 for WT and HDAC11 KO mice, respectively) or Δ*ddh/ldh1/ldh2* (n=10/group), whereupon bacterial burden in (**c**) implant-associated tissue and (**d**) femur was quantified at day 14 post-infection. (**e**) $CD11b^{high}Ly6G^{+}Ly6C^{+}$ MDSCs (**f**) $CD11b^{low}Ly6G^{+}Ly6C^{+}$ PMNs, (**g**) $Ly6G^{-}Ly6C^{+}F4/80^{-}$ monocytes, and (**h**) IL-10 were quantified in infected tissue at day 14 post-infection. Results represent the mean ± SEM combined from two independent experiments. (**i-k**) WT or Δ*ddh/ldh1/ldh2*-infected mice were treated with

vehicle or 0.5 mg/kg tubastatin A once daily, and sacrificed at day 14 post-infection for quantification of bacterial burden in (**i**) implant-associated tissue and (**j**) femur as well as (**k**) IL-10 in implant-associated tissues by ELISA. Results are (**i and j**) combined from three independent experiments (vehicle, n=21 and 22 for WT and Δ*ddh/ldh1/ldh2*, respectively; tubastatin A, n=22 and 21 for WT and Δ*ddh/ldh1/ldh2*, respectively) or (**k**) mean ± SD of one representative experiment (vehicle, n=5/group; tubastatin A, n=4 and 5 for WT and Δ*ddh/ldh1/ldh2*, respectively) performed two times. *, $p < 0.05$; **, $p < 0.01$; ***, $p < 0.001$; ****, $p < 0.0001$; One-way ANOVA. (**l**) During infection with wild type *S. aureus* (left panel), D- and L-lactate produced by the biofilm is transported into MDSCs and macrophages via the monocarboxylate transporter MCT1 where it inhibits HDAC11 activity. The lack of HDAC11 inhibition allows HDAC6-dependent IL-10 transcription to become unchecked, resulting in elevated IL-10 production. In the absence of *S. aureus* lactate (right panel), the inhibitory effect of HDAC11 on HDAC6 remains intact, which limits IL-10 production.

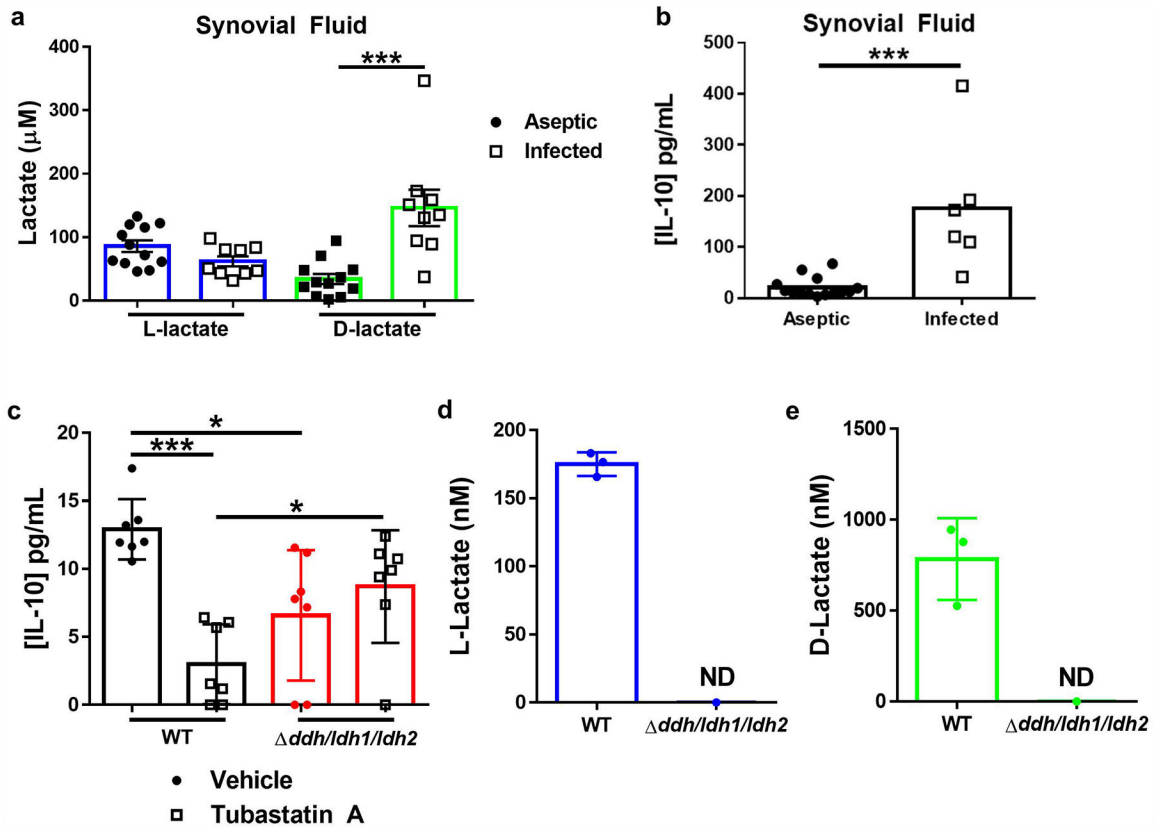

Figure 6. *S. aureus*-derived lactate induces IL-10 production by human monocyte-derived macrophages.

Synovial fluid samples from patients with PJI vs. aseptic loosening were examined for (**a**) L- and D-lactate (n=12 and 9 for aseptic and PJI, respectively; ***, $p = 0.0004$) and (**b**) IL-10 (n=14 and 6 for aseptic and PJI, respectively; ***, $p = 0.0003$). (**c**) Human monocyte-derived macrophages were co-cultured with clarified supernatants from WT or Δ*ddh/ldh1/ldh2* biofilm ± the HDAC6i tubastatin A (15 nM) for 2 h, whereupon IL-10 production was analyzed by ELISA. (**d**) L- and (**e**) D-lactate levels in clarified supernatants from WT or Δ*ddh/ldh1/ldh2* biofilm. Results represent (**c**) the mean ± SD from one representative experiment (n=7 biological replicates/group) repeated with monocytes from 3 different donors and (**d and e**) mean ± SEM from three independent experiments. ND, not detected. Results were analyzed by (**a and b**) an unpaired two-tailed Student's *t*-test and (**c**) One-way ANOVA (*, $p < 0.05$; ***, $p < 0.001$).